

Review

Review of the Photothermal Energy Conversion Performance of Nanofluids, Their Applications, and Recent Advances

Tsogtbilegt Boldoo¹, Jeonggyun Ham¹, Eui Kim¹ and Honghyun Cho^{2,*} 

¹ Department of Mechanical Engineering, Graduate school of Chosun University, Gwangju 61452, Korea; tsogtbilegt31@gmail.com (T.B.); orchiders@chosun.kr (J.H.); kkww2424@naver.com (E.K.)

² Department of Mechanical Engineering, Chosun University, Gwangju 61452, Korea

* Correspondence: hhcho@chosun.ac.kr; Tel.: +82-62-230-7050; Fax: +82-62-230-7055

Received: 26 September 2020; Accepted: 29 October 2020; Published: 2 November 2020



Abstract: Nanoparticles have been thoroughly investigated in the last few decades because they have many beneficial and functional qualities. Their capability to enhance and manipulate light absorption, thermal conductivity, and heat transfer efficiency has attracted significant research attention. This systematic and comprehensive work is a critical review of research on the photothermal energy conversion performance of various nanofluids as well as the recent advances in several engineering applications. Different nanofluids used in the photothermal energy conversion process were compared to identify the suitable applications of each nanofluid in thermal systems. An analysis of the previous investigations based on experimental and numerical studies has established that nanomaterials have the potential to increase the efficiency of solar thermal systems.

Keywords: nanofluid; photothermal energy conversion performance; solar thermal collector; thermal properties; thermal system

1. Introduction

In the last century, global industrialization has led human civilization to several beneficial ideas, such as infrastructure that connects countries, continents, or even planets and energy harvesting technologies that can be used to collect energy in various forms. However, such industrialization has also led to catastrophic events, natural resource depletion, sea-level rise, and global warming. Furthermore, it affects wildlife in forests worldwide, causing contagious diseases and epidemics. To decrease the acceleration of these catastrophic processes, 192 countries participated in the Kyoto Protocol [1], which was implemented to decrease the acceleration of global warming by significantly reducing the emission of greenhouse gases such as methane (CH₄), carbon dioxide (CO₂), nitrous oxide (N₂O), perfluorocarbons (PFCs), hydrofluorocarbons (HFCs), and sulfur hexafluoride (SF₆). The latest data in Figure 1 illustrate that the production of electricity and heat caused the emission of 13.4 billion tons of CO₂ [2] into the atmosphere, which is the highest in terms of manmade greenhouse gas emissions by sector.

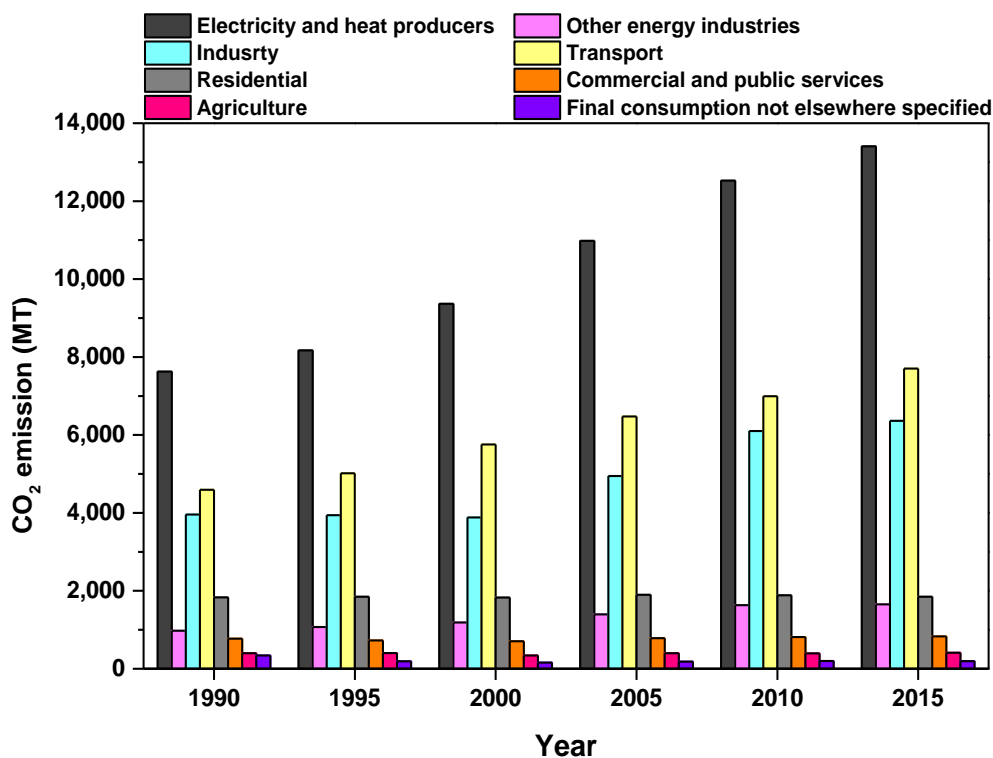


Figure 1. Global CO₂ emissions by sector [2]; 2018, IEA.

To meet the requirements of the Kyoto Protocol agreement and maintain the high speed of the development progress, many countries are in search of high-efficiency technologies, such as green technologies, which cause lower greenhouse gas emissions than previous-generation technologies and use renewable resources. Among the green and renewable-energy-based technologies, the harvesting of solar energy has attracted much research attention because an immense amount of energy (174,000 TW in the atmosphere) can be harvested with lower greenhouse gas emissions than any other method. However, solar energy harvesting technologies are less efficient than other technologies. Solar energy can be harvested by several different energy forms such as electricity, thermal, and chemical (fuels), and photothermal energy conversion processes can be used to obtain the heat [3]. According to the method of converting energy from sunlight, solar harvesting technologies can be divided into two main types: photovoltaic (PV) systems and solar thermal collectors. PV panels generate electric energy by absorbing solar energy via solar cells, which have an average efficiency of 15–17%. The technology for generating electricity using solar energy is widely used worldwide. In the case of solar thermal collectors, solar energy directly heats a working fluid, which can collect the heat in the solar collector for space and water heating. Conventional solar collectors have an average efficiency of 70%, but the efficiency varies according to the type of solar collector.

The most solar collectors use the photothermal energy conversion process that can achieve the highest conversion efficiency. The photothermal energy conversion mechanism is caused by the photoexcitation process that results in the thermal energy (heat) production by the materials. Moreover, energy from the sun is applied in the PV/T system and solar ponds. In the PV/T system, excessively absorbed heat from the PV module can utilize to heat the working fluid such as air and water [4]. In addition, those working fluids play a role as a coolant for solar cells, and which can improve the efficiency of PV because the overall efficiency of the solar cells hugely dependent on the operating temperature of PV panels. According to Dubey et al. [5] the power output of the PV module decreased with the increasing in operating temperature. Hence, applying a PV/T system is mutually beneficial for both the thermal and electrical system. In addition, one of the major challenges for researchers is to collect and properly storage solar thermal energy. The solar pond could be one of solutions to the

aforementioned problem [6,7]. The solar pond is generally consisted of multiple layers of salt solution and the concentration of the solution increased with the increase of pond depth.

Recently, researchers have started applying nanotechnology in solar thermal harvesting technologies to enhance the overall efficiency. At present, nanoparticles improve the overall thermal efficiency by enhancing the thermal properties of the working fluid in the solar thermal collector system. Nanofluids are a suspension of functionalized nano-sized materials (<100 nm) in a base fluid, which is a conventional working fluid such as water, oil, and ethylene glycol. Moreover, thermal and rheological properties can be easily controlled based on the manufacturing method and properties of the nanoparticles. Owing to their nanoscale particle size and large specific surface area, nanoparticles cause a significant increase in thermal conductivity. In addition, nanofluids can significantly increase the optical absorption efficiency according to their color and particle shape. By enhancing the thermal, rheological, and optical properties of the working fluid, the size of the entire heat transfer system can be notably reduced. These technologies have the potential for great economic benefits. To select a proper nanofluid for specific applications, many researchers comprehensively explore the thermos-physical and optical properties of various nanofluids. For example, when the nanofluid is used for the direct absorption solar collector (DASC), the thermal and optical properties of the nanofluid are comprehensively studied. In the DASC system, the nanofluid absorbs the solar energy directly from the sun through the transparent glass. Whereas, when the nanofluid is used for the surface absorption thermal collector, the optical properties of the nanofluid can be negligible. In the surface absorption thermal collector system, solar energy is firstly absorbed by the thermal conductive surface, and then transfers thermal energy to the nanofluid via conductive heat transfer. In addition, the economical factor should be considered depending on the scale of the application. Thus, this literature survey can help to choose proper nanofluid for specific applications.

Numerous articles have previously reviewed the properties of nanofluids and their applications in various engineering areas. However, the previous articles mainly focused on the use of nanofluids in solar thermal collectors but failed to summarize the critical property of photothermal energy conversion. This review article attempts to summarize the current state of research on the photothermal energy conversion of various types of nanofluids, as well as their use in different engineering applications. In addition, this article presents an extensive review of recent advances in the photothermal energy conversion of nanofluids and their efficiency in various engineering fields. To present a detailed perspective on the use of nanofluids in photothermal energy conversion technology, an overview of the important factors that affect the photothermal energy conversion performance of nanofluids is presented. Furthermore, this article discusses the present application range of photothermal energy conversion systems based on nanofluids and related advances. To increase the understanding of previous studies, related analyses and calculation techniques are illustrated. This article is expected to provide researchers with deep insight into the photothermal energy conversion of various nanofluids and facilitate future studies in this field.

2. Nanofluid Preparation for Solar Thermal Applications

A nanofluid is not simply a solid–liquid mixture; rather, it is a complex colloid formed by dispersing specific functionalized nanomaterials in conventional working fluids such as water, thermal oil, and refrigerants. One of the many problems faced by researchers working with nanofluids is the production of well-dispersed nanofluids. Owing to the interaction between neighboring nanoparticles, nanoparticles tend to agglomerate because of van der Waals forces [8]. In addition, because of the density difference between nanoparticles and the base fluid, nanoparticles tend to become sediment at the bottom of the nanofluid because of gravitational force. Furthermore, this aggregation and sedimentation of nanoparticles can significantly reduce the overall heat transfer efficiency of the system and can block the pump or contaminate the heat transfer area. Recent studies have shown that nanofluids tend to agglomerate under harsh operating conditions such as high temperature and pressure [9–11]. To manufacture nanofluids with good dispersion stability, researchers have used

surfactants as well as nanoparticle coating methods. The manufacturing method of nanofluids can be classified into two main groups: single-step and two-step manufacturing methods.

In the single-step manufacturing method, nanoparticle synthesis and dispersion in the base fluid are simultaneously performed using a physical vapor deposition technique or liquid chemical method. By avoiding drying, transportation, storage, and dispersion, a single-step manufacturing method reduces the chance of nanoparticle agglomeration or sedimentation in the nanofluid. Unfortunately, such methods cannot be used to manufacture nanoparticles at a large or industrial scale. The main concern when using the single-step method is the minimization of the residual chemical reagent in the nanofluid, which is a byproduct of an unstable chemical reaction and can reduce the purity level of the nanofluid.

The most widely used technique for manufacturing nanofluids in the industrial and research fields is the two-step method because it is economical and straightforward. In this method, nanomaterials such as nanoparticles, nanorods, nanofibers, and nanotubes are first manufactured in the form of a dry powder. As shown in Figure 2, nanoparticle synthesis methods are categorized into three groups: physical, chemical, and biological methods. Biological methods involve complicated processes and, hence, have not been broadly used. On the other hand, physical and chemical methods have been widely used and developed on research and industrial scales. Physical methods tend to use large devices, which require a tremendous amount of energy to operate, whereas chemical methods use simple techniques and have low energy consumption. After the nanoparticle synthesis, nanoparticles are mixed with the base fluid through ultrasonication, intensive magnetic stirring, homogenizing, high-shear mixing, and ball milling. The main drawback of the two-step method is the lack of dispersion stability. Therefore, surfactants and coating materials are broadly applied to stabilize the nanoparticles in the base fluid, and these materials can be used in a wide range of applications.

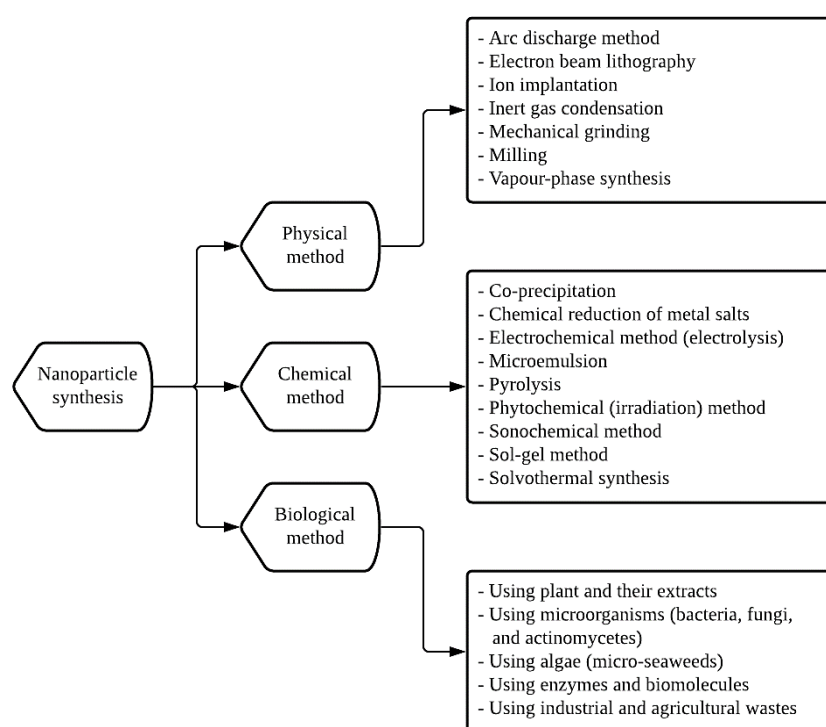


Figure 2. Classification of nanoparticle synthesis methods.

By summarizing some studies on the manufacturing of nanofluids, Table 1 [12–45] lists the synthesis methods of various nanofluids. As is evident from Table 1, the two-step manufacturing method is dominantly used in the research community. Owing to the high price and scarcity of gold, Au nanoparticles are usually synthesized using one-step methods. Furthermore, owing to

the dispersion stability, most nanofluids used surfactants, which vary according to the base fluid and nanoparticles. In studies that used a one-step synthesis method, nanoparticles did not require additional surfactants or coating; however, studies that used metal oxides mostly required surfactants. In addition, DI water and ethylene glycol have been extensively used as the base fluid in nanofluids because of their favorable thermal properties, low viscosity, and low toxicity. Ethylene glycol and its mixture with DI water were used in experimental studies because of their low freezing point. In some harsh operation conditions, the heat transfer system requires a lower freezing point than DI water. Nevertheless, the use of ethylene glycol alone in the heat transfer system is not a good choice because of its high viscosity, which is why most of the studies used its mixture with DI water.

Table 1. Synthesis methods of nanofluids.

Ref.	Nanoparticles	Manufacturing Method	Base Fluid	Concentration	Surfactant
[12]	Al ₂ O ₃ , Co ₃ O ₄	two-step	DI water	40–230 mg/L	Triton X-100
[13]	Fe ₃ O ₄ , TiO ₂ , Fe ₃ O ₄ @TiO ₂	two-step	DI water	0.1 g/L	-
[14]	Multi-walled carbon nanotube (MWCNT), SiO ₂ /Ag, MWCNT-SiO ₂ /Ag	two-step	DI water	0.001–0.1vol%	-
[15]	CuS	two-step	DI water	0.002–0.02vol%	-
[16]	MrGO	two-step	DI water	0.5–2 mg/L	-
[17]	Fe ₃ O ₄	two-step	DI water	0.05wt%	SDS
[18]	Ag, Cu, Zn, Fe, Si, Al ₂ O ₃	two-step	DI water	0.01wt%	Trisodium citrate
[19]	Au	one-step	DI water	25–10 mg/L	-
[20]	Au, CNT, Fe ₃ O ₄	two-step	DI water	10–50 ppm	-
[21]	Fe ₃ O ₄	two-step	Water	1–5wt%	-
[22]	Graphite	two-step	DI water/Paraffin	-	-
[23]	Au, MWCNT	two-step	DI water	0.0001–0.004vol%	-
[24]	rGO, Ag-rGO	two-step	DI water	10–100 mg/L	-
[25]	CuO	two-step	Paraffin	0.01–0.1wt%	SSL
[26]	TiN, Au/TiN	two-step	EG	10–100 ppm	-
[27]	CuO-MWCNT	two-step	DI water	0.01–0.25wt%	-
[28]	CB	two-step	Paraffin wax-hexadecene	0–2.5wt%	-
[29]	CB	two-step	EG	2–15 ppm	PVP-K30
[30]	Ag-Au/Nitrogen doped graphitic polyhedrons (ZNG), Au/ZNG, ZNG	two-step	EG	10–100 ppm	-
[31]	RGO- α -Fe ₂ O ₄	two-step	EG	0.001–0.007wt%	PVP-K30
[32]	Fe ₂ O ₃	two-step	DI water	64–321 mg/L	Tween 80
[33]	AgNO ₃	two-step	DI water	0.05–10vol%	PVA
[34]	Au	one-step	DI water	1–125 ppm	-
[35]	Fe ₃ O ₄ , Cu, Au, Fe ₃ O ₄ + Cu, Fe ₃ O ₄ + Au, Cu + Au, Fe ₃ O ₄ + Cu + Au	two-step	DI water	3–15 ppm	Trisodium citrate
[36]	RGO, Ag, RGO@Ag	two-step	DI water	0.225–1 mg/mL	-
[37]	Fe ₃ O ₄	two-step	DI water	0.5–3 wt%	-
[38]	Au, Ag	-	DI water	0.0001 wt%	-
[39]	MWCNT, Fe ₃ O ₄ , MWCNT/Fe ₃ O ₄	two-step	DI water/EG	0.005–0.2 wt%	Citric acid
[40]	MWCNT	two-step	DI water	0.005–0.05 wt%	SDS
[41]	MWCNT, Fe ₃ O ₄ , MWCNT/Fe ₃ O ₄	two-step	DI water/EG	0.005–0.2 wt%	PAA
[42]	Co ₃ O ₄	-	DI water	5–30 mM	-
[43]	Au	one-step	DI water	0.00028–0.0112 wt%	-
[44]	Au	one-step	DI water	5–178 ppm	-
[45]	Au	one-step	DI water	0.008–0.04 wt%	-

In the next section, the optical properties and photothermal energy conversion performance of various nanofluids are discussed and illustrated.

3. Optical Properties of Nanofluids

The optical properties of nanofluids, including the optical transmittance, scattering, extinction coefficient, and solar weighted absorption fraction, play an important role in the photothermal energy conversion of a heat transfer system. The optical properties of nanofluids can be modified by controlling the nanoparticle size, concentration, and morphological properties. According to Gao et al. [3], the photothermal energy conversion mechanism is categorized depending on their corresponding light absorption range as plasmonic localized heating, non-radiative relaxation in semiconductors, and thermal vibration in molecules.

The plasmonic photothermal energy conversion can be observed when metallic nanoparticles irradiated with their resonance wavelengths, which is shown in Figure 3. When semiconductors illuminated, excited electrons in semiconductors generate energy near the bandgap energy. Moreover, generated energy is discharged in phonon form, which produces the local heating. In the case of thermal vibration driven photothermal energy conversion process, organic materials convert its absorbed energy from solar energy to lattice vibration, which excites the electrons in the materials.

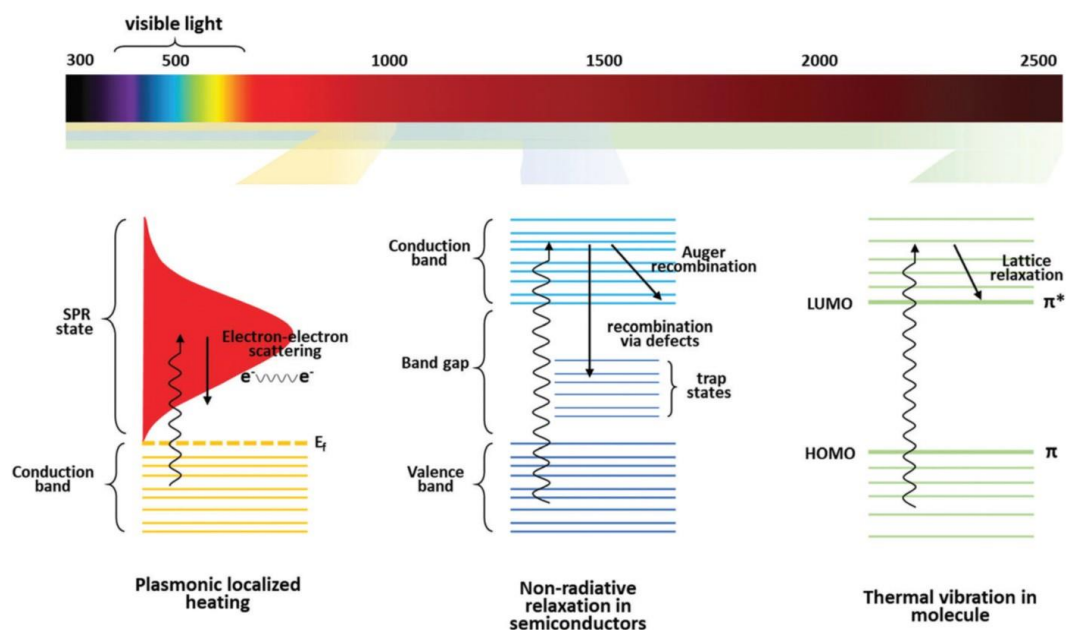


Figure 3. Different mechanisms of the photothermal effect with the corresponding light absorption range [3]; 2018, RSC.

The optical absorption of plasmonic metal nanoparticles is governed by the localized surface plasmonic resonance effect, which is strongly dependent on the size, shape, and fluid around the nanoparticles. To further improve their optical absorption properties, dielectric environment modification, structural engineering, and nanoparticles arrangements are generally used. One of the challenges of using the plasmonic metal nanoparticles is to decrease the limited absorption wavelength range for each nanoparticle, which is shown in Figure 4.

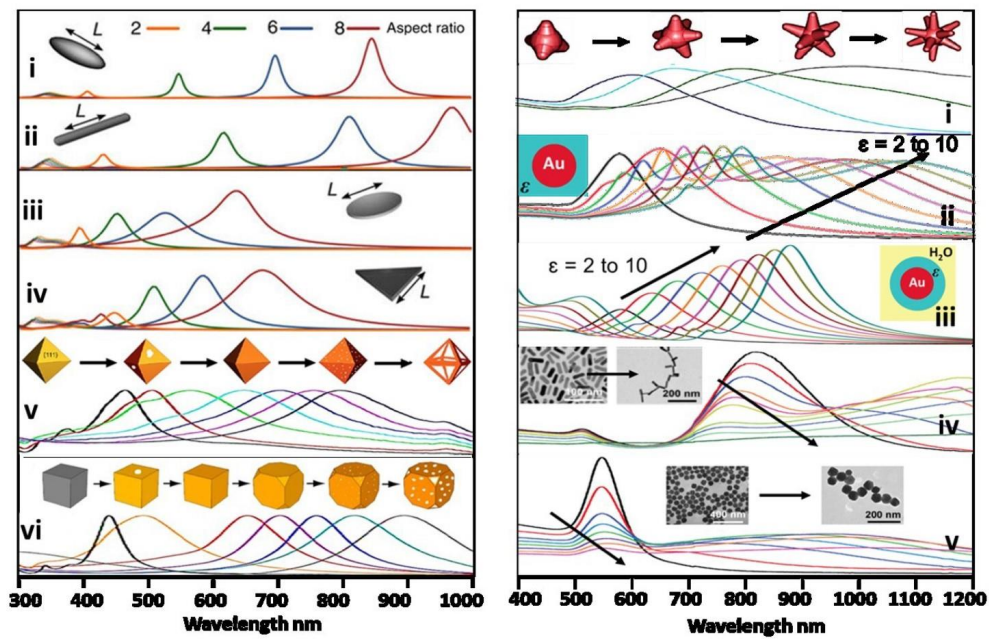


Figure 4. The change of optical absorption of plasmonic metals with the influence of structural tuning [3]; 2018, RCS.

When a fluid containing nanoparticles interacts with photons or electromagnetic waves, the nanoparticles decrease the transmittance by absorbing or scattering the photons or electromagnetic waves, as shown in Figure 5 [46]. The optical transmittance of a nanofluid is the fraction of light transmitted through the nanofluid sample. Figure 6 schematically shows "light radiation of radiant power", P_0 , directly beamed into a nanofluid sample. Owing to the absorption of the sample, the light radiation power was reduced to P . The optical transmittance of the sample can be calculated using Equation (1):

$$\%T = \frac{P}{P_0} \cdot 100 \tag{1}$$

where P_0 and P are the light radiation power before and after the absorption, respectively. The absorption of samples can be calculated using the optical transmittance, as expressed in Equation (2):

$$A = \lg P_0/P = \lg 100/\%T \tag{2}$$

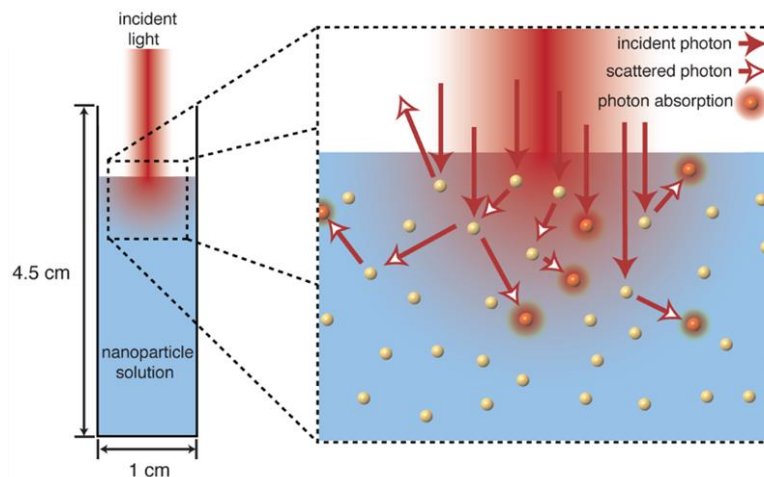


Figure 5. Schematic illustration of light scattering and absorption [46]; 2014, ACS.

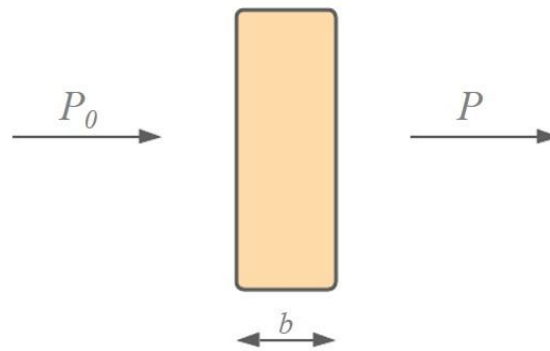


Figure 6. Schematic of light transmittance and absorbance.

Taylor et al. [47] reported that water as a base fluid is a good absorber at long wavelengths; it is also a good emitter at the same wavelengths. Hence, additional nanoparticles in the base fluid (water) could be the ideal compensation for the decrease in emission at longer wavelengths. Furthermore, the results of their work suggest that light scattering is negligible when the particle size is less than 50 nm. However, a measurable amount of light can be scattered if the particle size is >50 nm or a particle cluster exists. They also reported that the incoming solar radiation is absorbed by the thin top layer of the nanofluid at an excessive nanoparticle concentration, leading to thermal loss to ambient air. On the other hand, if the nanofluid concentration is too low, the nanofluid cannot absorb an appropriate amount of solar energy. As shown in Figure 7, Fang et al. [48] reported that the colors of CuO, ZnO, and CuO/ZnO nanofluids became darker as the nanofluid concentration increased. Moreover, the light absorption of the nanofluid increased as the color became darker. Vijayanandan et al. [42] studied the optical and photothermal energy conversion of a Co_3O_4 nanofluid synthesized by the endophytic fungus *Aspergillus nidulans*. They reported that nanoparticles with a diameter smaller than the incident wavelengths interacted with the light irradiation through Rayleigh scattering.

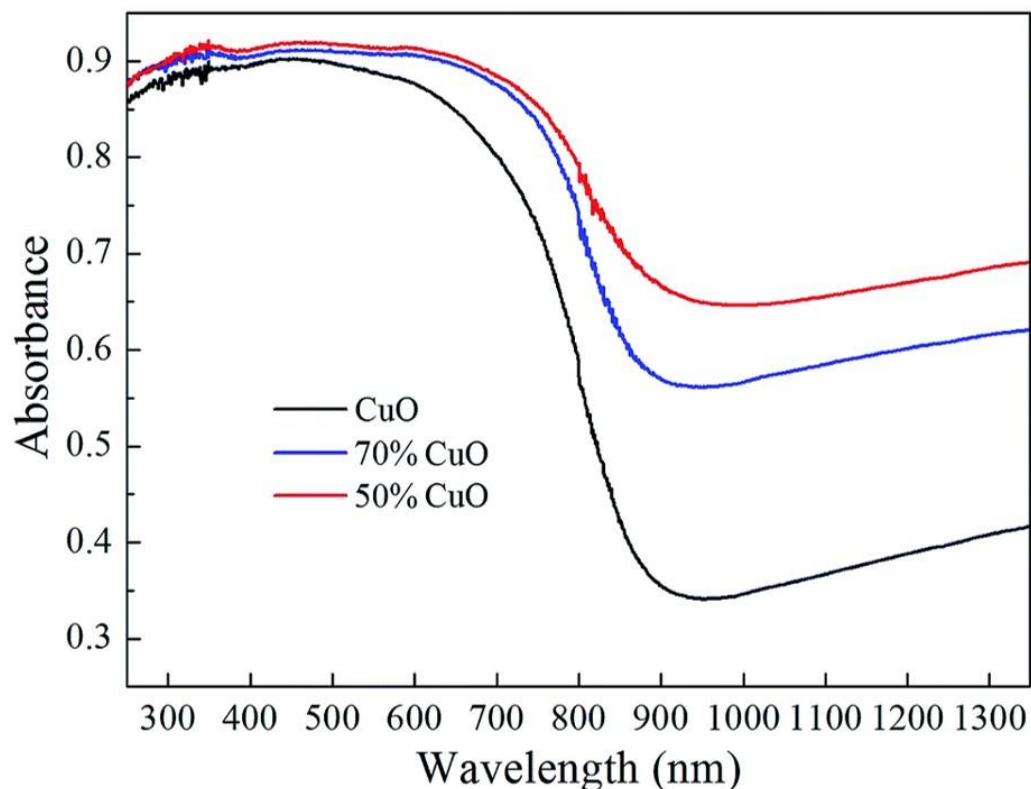


Figure 7. Diffuse reflection absorbance of CuO nanofluid [48]; 2017, RSC.

The existing open literature indicates that the optical transmittance of nanofluids generally decreases with an increase in nanofluid concentration [49–52]. The transmittance of pure water is close to zero at a wavelength of 1370–2500 nm, which implies near-perfect absorption in the near-infrared spectral range [49,51]. However, nanofluids have a much lower transmittance than pure water in the wavelength range of 250–1370 nm, as shown in Figure 8.

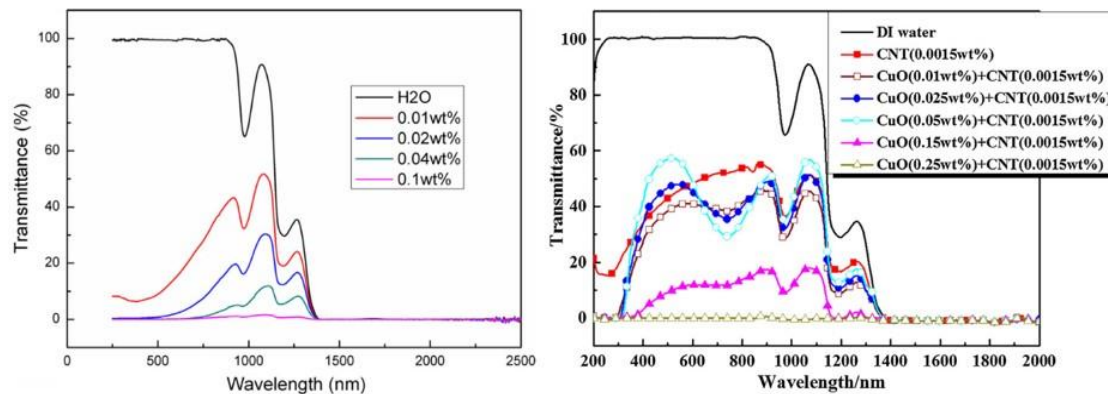


Figure 8. Optical transmittance of nanofluids [49,51]; 2017, 2013, Elsevier.

By introducing representative studies related to the optical properties of nanofluids, Tong et al. [39] and Shin et al. [41] experimentally investigated the optical transmittance of Fe_3O_4 , multi-walled carbon nanotubes (MWCNTs), and MWCNT/ Fe_3O_4 hybrid nanofluids. In their experiments, the maximum optical transmittance of the Fe_3O_4 nanofluid decreased by approximately 5% when the nanofluid concentration increased from 0 to 0.005 wt% at a wavelength of 750 nm. However, the incident light was completely absorbed when the concentration of the Fe_3O_4 nanofluid reached 0.2 wt%. A similar trend was observed in the MWCNT and MWCNT/ Fe_3O_4 hybrid nanofluids.

The solar weighted absorption coefficient of a nanofluid defines the fraction of solar energy absorbed by a given thickness of the nanofluid layer, and it is calculated using Equation (3):

$$A_m = \frac{\int_{\lambda_{\min}}^{\lambda_{\max}} S_m (1 - e^{-k(\lambda)x}) dx}{\int_{\lambda_{\min}}^{\lambda_{\max}} S_m(\lambda) d\lambda} \quad (3)$$

where S_m and $k(\lambda)$ are the spectral solar irradiance in the atmosphere (AM1.5 solar spectrum) and extinction coefficient as a function of the given wavelength, respectively. It can be noted from Equation (3) that the solar weighted absorption coefficient is primarily dependent on the extinction coefficient of the nanofluid. Moreover, the extinction coefficient of the nanofluid is strongly dependent on the type of nanomaterial and the volume or mass fraction. Du et al. [53] revealed that the effect of optical scattering could be negligible when nanoparticles are seriously aggregated in a nanofluid. Hence, conventional Rayleigh or Mie theories cannot be employed to predict the optical properties of nanofluids. Furthermore, they found that particle agglomeration could improve the extinction coefficient of nanofluids at a long wavelength while insignificantly reducing the optical absorption. In addition, an increase in the nanoparticle size can result in an enhancement of the extinction coefficient.

In the design of a solar thermal harvesting system, the calculation of the solar weighted absorption fraction plays an important role in achieving a high efficiency. A previous investigation on the solar weighted absorption coefficient showed that the penetration distance decreases with an increase in the nanofluid concentration [12,19,32,54]. Qu [27] reported that the solar absorption fraction of CuO nanofluid rapidly increased with an increase in the nanofluid concentration at a penetration distance of 1 cm, as shown in Figure 9. The solar weighted absorption fraction of the 0.25 wt% CuO nanofluid

reached 90% at a penetration distance of 1 cm; however, the solar weighted absorption fraction of 0.01 wt% CuO nanofluid did not even reach 70% at a penetration distance of 10 cm. Water, the base fluid, has a high optical transmittance and, consequently, a solar weighted absorption fraction of only 25% at a penetration distance of 10 cm. In addition, Zhu et al. [55] explained the photothermal energy conversion mechanism. When the surface of the matter exposed to electromagnetic irradiation, a portion of the photon energy can convert into other forms of energy such as thermal energy, which can be observed in the Figure 10.

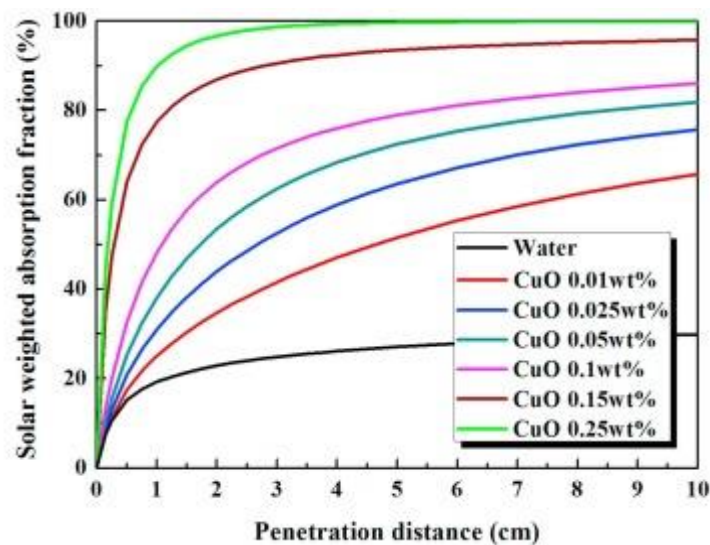


Figure 9. Solar weighted absorption fraction of CuO nanofluid with different nanofluid concentrations [27]; 2018, Elsevier.

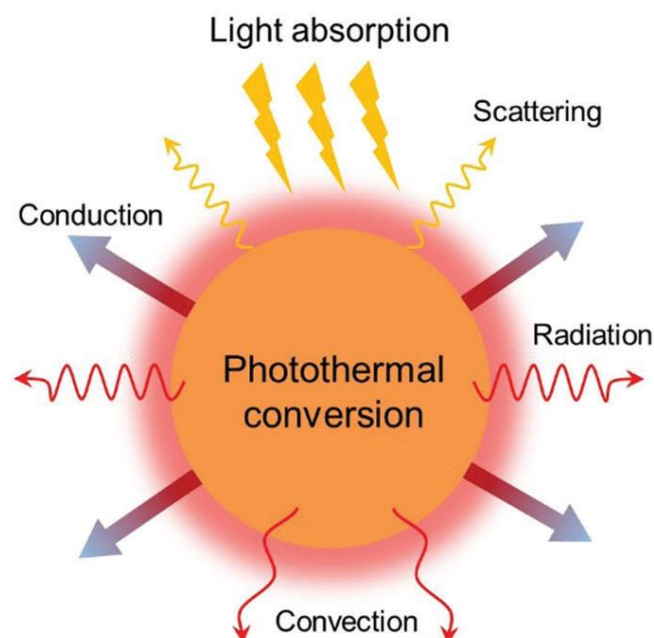


Figure 10. Photothermal energy conversion mechanism by Zhu et al. [55]; 2018, RCS.

It can be deduced from the aforementioned studies that additional nanoparticles increase the absorption of the working fluid by decreasing the optical transmittance. When nanoparticles are added to the working fluid, the optical absorption wavelength range increases beyond that of fully

transparent working fluids such as water and ethylene glycol. This phenomenon is advantageous for applying nanofluids to photothermal energy conversion devices.

4. Photothermal Energy Conversion Performance of Nanofluids

To investigate the photothermal energy conversion performance of the working fluid, many researchers [23,28,37,42,48,56] utilized the photothermal energy conversion efficiency and specific absorption rate of the working fluid. For instance, the photothermal energy conversion efficiency can be calculated using Equation (4) [27]:

$$\eta = \frac{(c_{bf}m_{bf} + c_{nf}m_{nf})}{IA\Delta T} \approx \frac{c_{bf}m_{bf}}{IA} \cdot \frac{\Delta\bar{T}}{\Delta t} \quad (4)$$

where c_{bf} , m_{bf} , c_{nf} , and m_{nf} are the specific heat and mass of the base fluid and nanofluid, respectively; I and A are the solar incident irradiance and exposure area to the solar source, respectively; $\Delta\bar{T} = \Delta T_{tc1} + \Delta T_{tc2} + \Delta T_{tc3}$ is the average temperature increase; and Δt is the exposure time to the solar source. Moreover, the specific absorption rate (SAR) can be calculated to determine the capacity of the nanoparticles to absorb energy within a given time, and it can be expressed as Equation (5) [27]:

$$SAR = \frac{(c_{bf}m_{bf} + c_{nf}m_{nf})\Delta\bar{T}_{nf} - c_{bf}m_{bf}\Delta\bar{T}_{bf}}{m_{nf}\Delta t} \quad (5)$$

Hogan et al. [46] investigated heating through light localization of nanoshell (NS) and nanomatryoshkas (NM), which have a similar optical absorption through cross-section of $1 \times 10^{-10} \text{ cm}^2$ at a wavelength of 808 nm. Figure 11 shows their simulation results for temperature distributions over time in nanofluid samples. The geometry was modeled using the 3D thermal transport finite element method (FEM, Cosmol). The temperature was calculated at the top, middle, and bottom parts of the samples. They assumed that convective heat transfer along the axis of light irradiation could be negligible owing to the temperature distribution in the nanofluid sample.

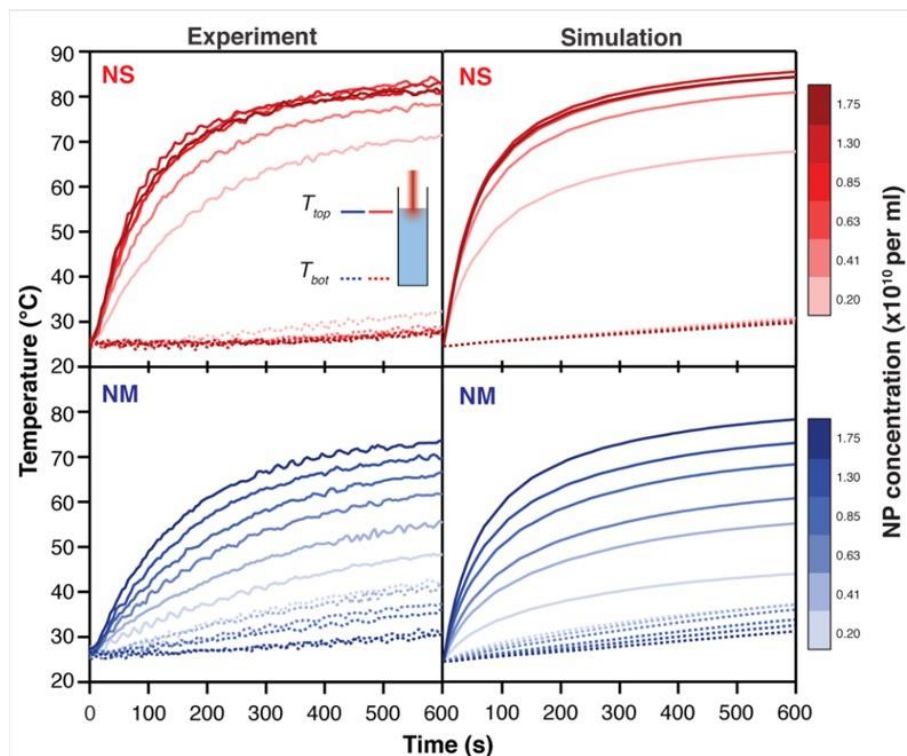


Figure 11. Numerical result of the temperature distribution in nanofluids [46]; 2014, ACS.

Table 2 lists the photothermal energy conversion performance of different nanofluids by comparing their temperature rises [23,42,43,51,57–61]. In addition to the nanofluid properties, the differences in temperature rise can be caused by differences in the exposure time or light source and solar irradiance intensity. Fang et al. [48] studied the optical and photothermal energy conversion performance of binary CuO/ZnO nanofluid. They noticed that the photothermal energy conversion efficiency of CuO nanofluid could be enhanced from 95% to 97.35% by adding ZnO nanoparticles (Cu/ZnO = 7/3). In the comparative study of Amjad et al. [45], Al₂O₃- γ , Si, Cu, Zn, Fe, and Ag nanofluids exhibited significant enhancements in the photothermal energy conversion performance, and the Ag nanofluid exhibited the best result amongst all the nanofluids, as shown in Figure 12. Zeng et al. [24] examined the photothermal energy conversion performance of an MWCNT-SiO₂/Ag binary nanofluid. As shown in Figure 13, the binary MWCNT-SiO₂/Ag nanofluid has a significantly higher photothermal energy conversion performance than the unitary SiO₂/Ag nanofluid. The photothermal energy conversion efficiency of all the nanofluids decreased owing to the high temperature at the top upper part of the nanofluid. Chen et al. [57] studied the sunlight absorption performance of Ag nanofluids under simulated and natural sunlight. As shown in Figure 14a, owing to the plasmonic effect of the Ag nanofluid, the maximum temperature was observed in the nanofluid with 80.94 ppm Ag, even though the nanofluid containing the semiconductor ZnO had a higher nanofluid concentration under the same simulated sunlight. Optical scattering and absorption can significantly improve under the resonance light condition. It is also clear from Figure 14b that the temperature rise of the Ag nanofluid is much higher than that of water.

Table 2. Temperature rise achieved for various nanofluids [36]; 2019, Elsevier.

Ref.	Nanofluid	Temperature Increase, °C		Light Source	Exposure Time
		Nanofluid	Base Fluid		
[51]	Cu	17.7	14.12	Sunlight	23,000 s
[57]	Al ₂ O ₃	9	-	-	18 min
[58]	TiO ₂ /Ag	30	20	Sunlight	8 h
[59]	Ag	10	1	Sunlight	10 h
[43]	Au	13	8	Simulator	5 min
[60]	Graphene	25	-	Simulator	1200 s
[61]	Ag	18	16	Simulator	60 min
[23]	Gold, MWCNT	33.1, 43.5		Sunlight	3 h
[42]	Biosynthesized Co ₃ O ₄	16.66	12	Sunlight	90 min

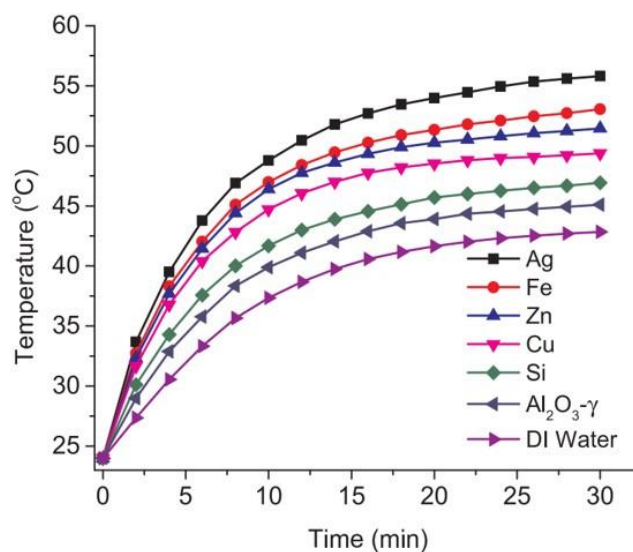


Figure 12. Variation of temperature versus time for various nanofluids [18]; 2020, Elsevier.

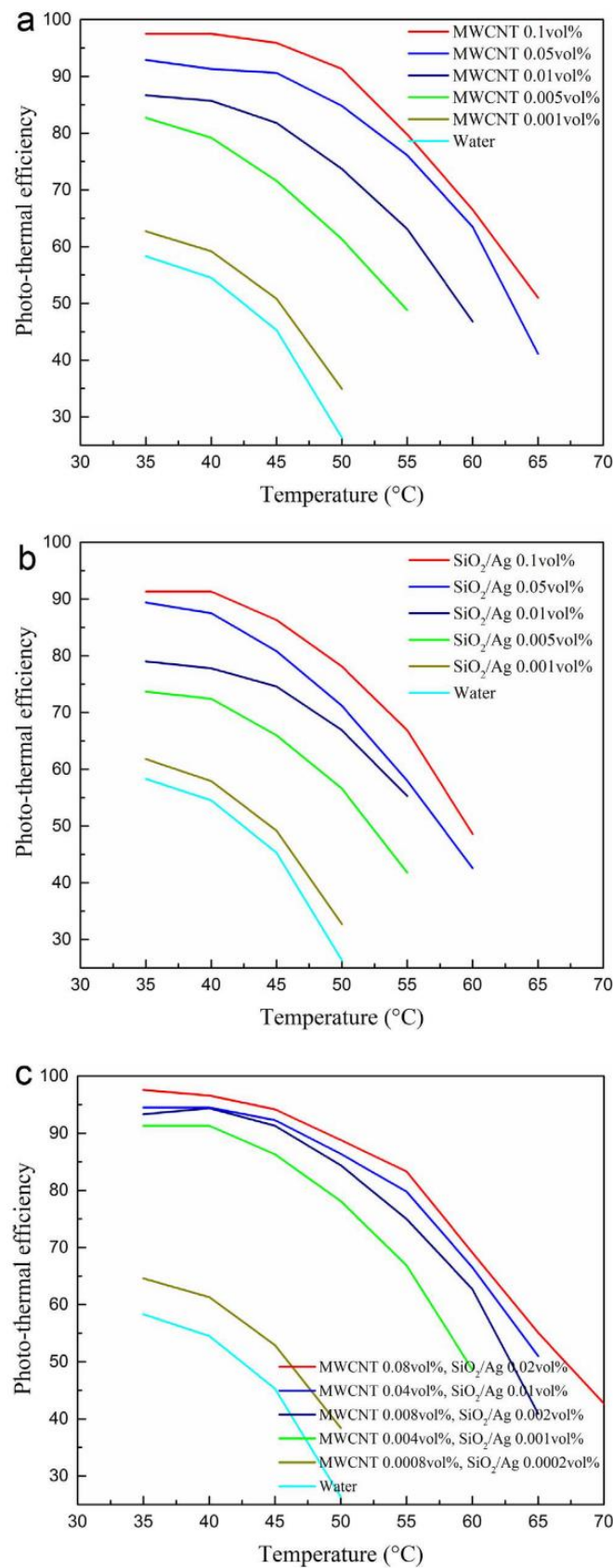


Figure 13. Calculated photothermal efficiency of nanofluids: (a) multi-walled carbon nanotubes (MWCNT) nanofluids, (b) SiO₂/Ag nanofluids, and (c) binary nanofluids with MWCNT:SiO₂/Ag = 4:1 [14]; 2018, Elsevier.

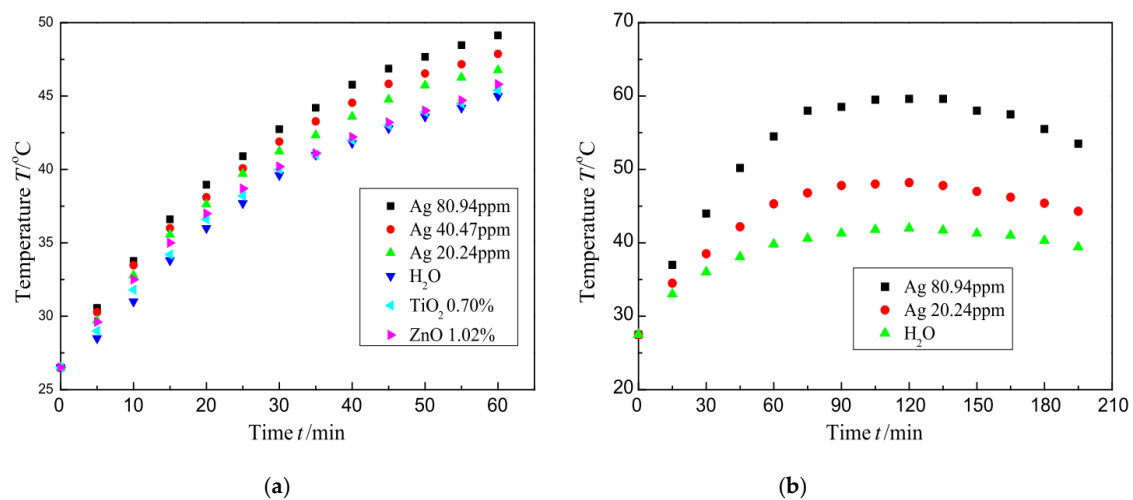


Figure 14. Characteristic curve of the temperature rise of nanofluids under (a) simulated and (b) natural sunlight conditions [61]; 2018, IOSR.

According to Meng et al. [62], the heat emission from a Carbon nanotube (CNT) nanofluid to the surrounding air increased when the nanofluid sample was heated by a solar source. The equilibrium temperature of the sample represented the photothermal energy conversion efficiency, and the photothermal energy conversion efficiency was enhanced with increasing equilibrium temperature. Moreover, the equilibrium temperature of the CNT nanofluid increased with increasing CNT nanofluid concentration. For example, the equilibrium temperature increased by 14.6 °C for a nanofluid with 4.0 wt% CNT, which is 42% higher than that of the base fluid (pure ethylene glycol). Furthermore, their results revealed that the CNT nanofluid had a higher photothermal energy conversion performance than the water-based TiO₂ and SiO₂ nanofluids under identical experimental conditions. Zhu et al. [30] studied the photothermal energy conversion performance of bimetallic Ag–Au alloys in nitrogen-doped graphitic polyhedrons (ZNGs) because of the plasmonic effect of Ag and Au as well as the unique optical spectral absorption of carbon materials. According to Figure 15a, all ethylene-glycol-based nanofluids exhibited the same increasing trend of temperature. Owing to the equilibrium temperature of each nanofluid, different maximum temperatures were observed depending on the type of nanofluid. The photothermal energy conversion efficiency of the Ag–Au/ZNG nanofluid was 74.35% and 38.71% at concentrations of 100 and 10 ppm, respectively. Tong et al. [39] experimentally investigated the photothermal energy conversion performance and efficiency of Fe₃O₄ and hybrid MWCNT/Fe₃O₄ nanofluids at different weight mixing ratios such as 1/4, 2/3, 3/2, and 4/1. Their photothermal energy conversion experiment consisted of two stages: a heating stage and an energy-absorbing stage. In the heating stage, the temperature of the sample increased with the exposure time. Once the temperature reached the equilibrium temperature, the heat loss from the working fluid to ambient air would be equivalent to the energy obtained from the light source in the working fluid, which was the second stage in the photothermal energy conversion process. In the energy-absorbing stage, the energy absorbed by the sample is equal to the heat loss to ambient air owing to the high temperature of the sample. Hence, the temperature of the samples remained constant.

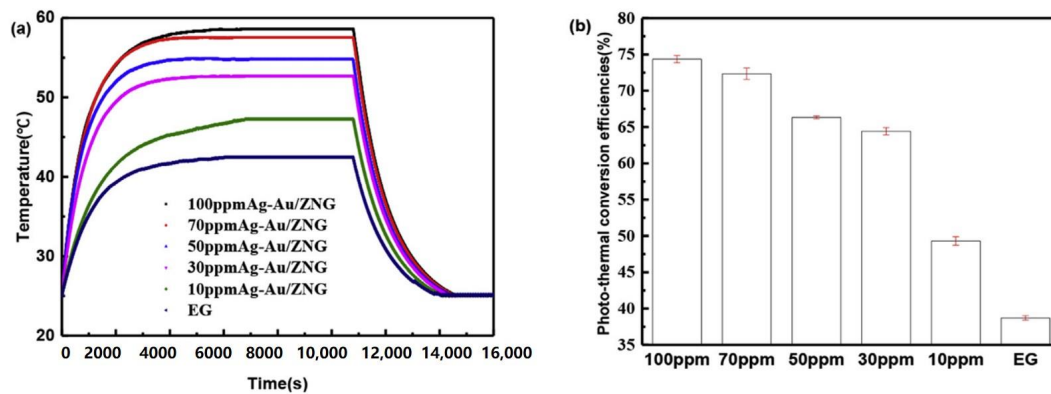


Figure 15. (a) Temperature variation and (b) photothermal energy conversion efficiency of Ag–Au/Nitrogen doped graphitic polyhedrons (ZNG) nanofluid with various concentrations [30]; 2019, Elsevier.

To improve the heat transfer performance in solar collecting systems, various studies have attempted to apply magnetic nanofluids. Boldoo et al. [63] reported that the photothermal energy conversion of Fe_3O_4 nanofluid showed a promising improvement under an external magnetic field. At the same Fe_3O_4 nanofluid concentration of 0.2 wt% and magnetic field intensity of 750 Gauss, the maximum temperatures in the absence and presence of the magnetic field were 46.4 °C and 51.3 °C, respectively. Zeng et al. [64] theoretically and experimentally studied magnetic and plasmonic $\text{Fe}_3\text{O}_4/\text{TiN}$ nanofluids. Both studies showed that the $\text{Fe}_3\text{O}_4/\text{TiN}$ nanofluid reached full-spectrum optical absorption. Furthermore, the optical absorption of the $\text{Fe}_3\text{O}_4/\text{TiN}$ nanofluid decreased with increasing magnetic field intensity. However, the thermal conductivity of the $\text{Fe}_3\text{O}_4/\text{TiN}$ nanofluid increased when the magnetic field direction was aligned with the nanofluid heat transfer direction. The formation of a chain-like nanoparticle cluster in the nanofluid under an external magnetic field could cause this phenomenon. Shin et al. [41] reported that the photothermal energy conversion performance of a magnetic nanofluid increased under an external magnetic field. As shown in Figure 16, the temperature increase of the 0.2 wt% $\text{MWCNT}/\text{Fe}_3\text{O}_4 = 1/1$ hybrid nanofluid increased with increasing magnetic field intensity. The final temperatures of the 0.2 wt% $\text{MWCNT}/\text{Fe}_3\text{O}_4 = 1/1$ hybrid nanofluid increased from 45 °C to 60 °C when the magnetic intensity increased from 0 to 750 Gauss. They assumed that the improvement in the photothermal energy conversion performance of the $\text{MWCNT}/\text{Fe}_3\text{O}_4$ hybrid nanofluid was caused by the chain-like structure of Fe_3O_4 nanoparticles in the nanofluid. Moreover, the stored energy in the $\text{MWCNT}/\text{Fe}_3\text{O}_4$ hybrid nanofluid increased with increasing magnetic intensity. Figure 17 shows the total stored energy in the 0.2 wt% $\text{MWCNT}/\text{Fe}_3\text{O}_4$ hybrid nanofluid during heating under different magnetic intensities.

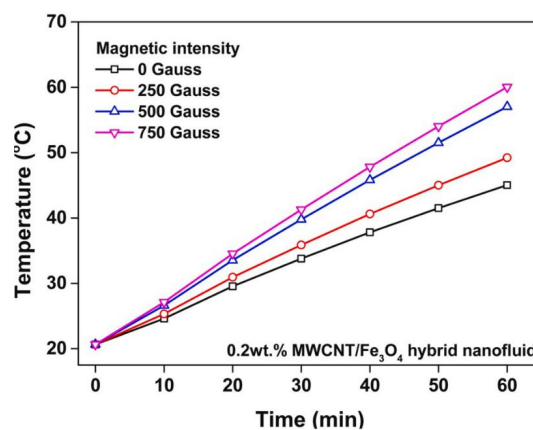


Figure 16. Variation of temperature with time for the 0.2 wt% $\text{MWCNT}/\text{Fe}_3\text{O}_4$ hybrid nanofluid under different magnetic intensities [41]; 2020, Elsevier.

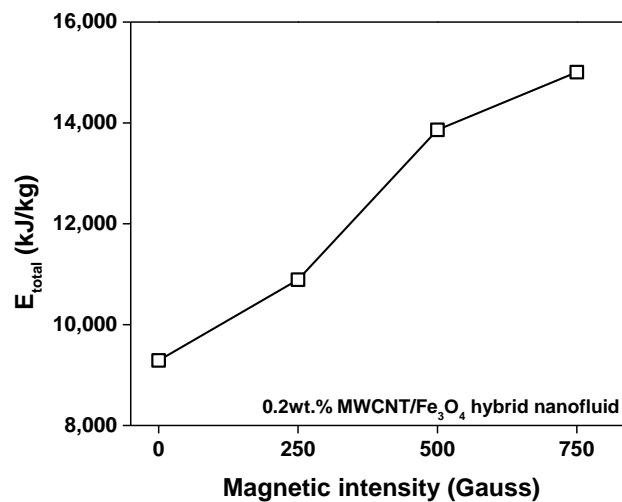


Figure 17. Total stored energy in a 0.2 wt% MWCNT/Fe₃O₄ hybrid nanofluid during heating under different magnetic intensities [41]; 2020, Elsevier.

In the review article of Verma et al. [65], the photothermal energy conversion efficiency increased with an increase in the particle concentration up to an optimal concentration, beyond which the nanoparticles agglomerated or formed some clusters in the nanofluid. Furthermore, the optical absorption of smaller nanoparticles tended to peak in the UV-Vis region, while larger particles absorbed at longer wavelengths. Chen et al. [66] observed a sudden drop in the photothermal energy conversion efficiency of GO/water nanofluid at concentrations of 0.05 wt% and 0.1 wt%, as shown in Figure 18c. They assumed that the drop was caused by agglomerated GO sheets formed at elevated temperatures, as indicated by Figure 18a,b. According to Figure 18a,b, the optimal nanofluid concentration of GO/water was 0.2 wt%, at which the nanofluid exhibited good dispersion stability and a high photothermal energy conversion efficiency; however, the absolute zeta potential decreased when the concentration increased from 0.02 wt% to 0.1 wt%. Moreover, the dispersion stability of the GO/water nanofluid significantly decreased with increasing temperature at all nanofluid concentrations. Liu et al. [67] investigated the dispersion stability of 1-Methylimidazolium tetrafluoroborate ([HMIM]BF₄) ionic liquid-based modified graphene (MGE/[HMIM]BF₄) nanofluid with 500 heating–cooling cycles (30 °C–180 °C, 180 °C–30 °C) over one month; such cycling can be applied in a photothermal energy conversion experiment. Figure 19a shows the unheated and heated MGE/[HMIM]BF₄ nanofluid. The MGE/[HMIM]BF₄ nanofluids exhibited good dispersion stabilities after heating at 180 °C for one month, except for the 0.01% MGE/[HMIM]BF₄ nanofluid, as shown in Figure 19b. The authors attributed the good dispersion stability of the MGE/[HMIM]BF₄ nanofluid to the good combination of the [HMIM]BF₄ ionic liquid and graphene modification. In addition, Boldoo et al. [68] compared the photothermal energy conversion performance of COOH-functionalized and non-functionalized MWCNT nanofluids. They found that the COOH-functionalized MWCNT nanofluid exhibited superior photothermal energy conversion performance than the non-functionalized MWCNT nanofluid at the same nanofluid concentration owing to the enhancement of stability. Wang et al. [44] reported that the evaporation rate of Au plasmonic nanofluid is significantly enhanced with increasing nanofluid concentration because of sunlight, as shown in Figure 20a,b. The high evaporation rate was caused by the highly concentrated Au nanofluid, which exhibited strong optical absorption; however, the highly concentrated Au nanofluid exhibited low specific vapor productivity (SVP) values because of the low optical transmittance, implying that the lower part of the nanofluid cannot interact with sunlight. Meanwhile, the significant amount of nanoparticles at the lower part of the nanofluid had nearly no chance to perform the photothermal energy conversion process for steam generation.

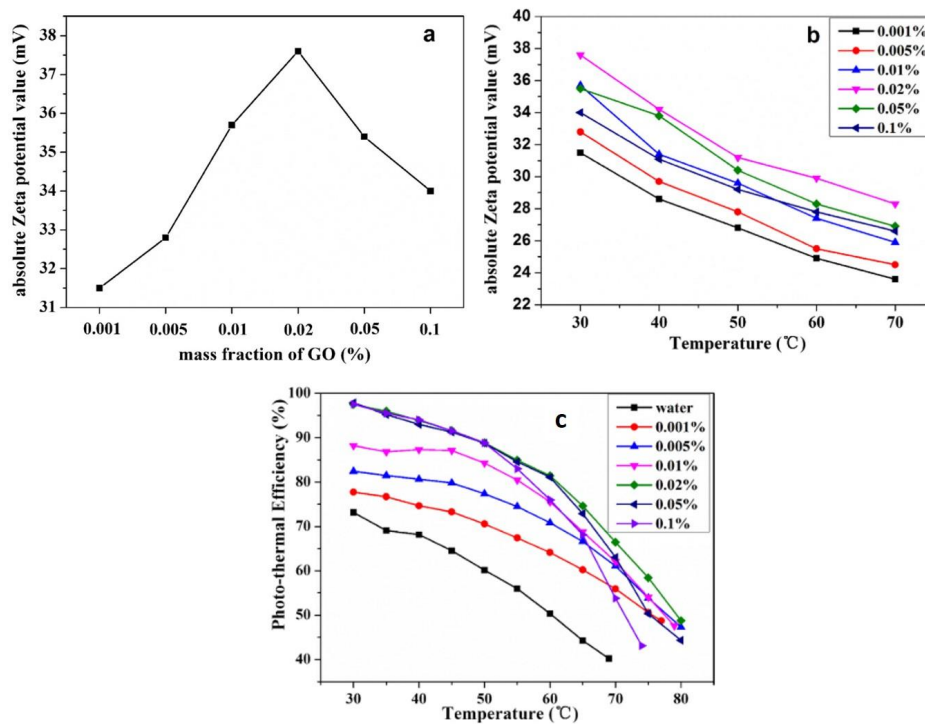
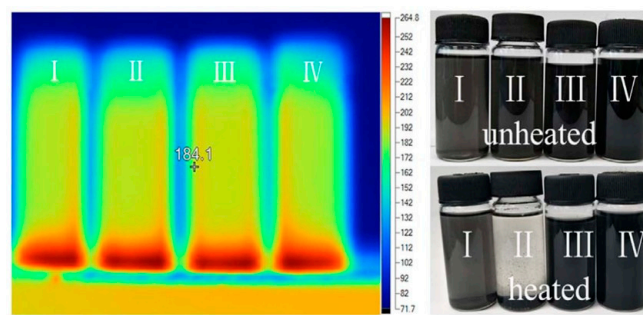
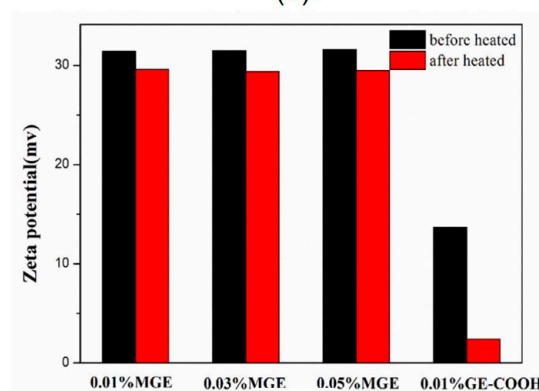


Figure 18. (a,b) Zeta potential and (c) photo-thermal energy conversion of GO/water nanofluid [66]; 2017, Elsevier.



(a)



(b)

Figure 19. (a) Infrared thermography and photographs and (b) zeta potentials of nanofluids before and after being kept at 180 °C for one month [67]; 2017, Elsevier.

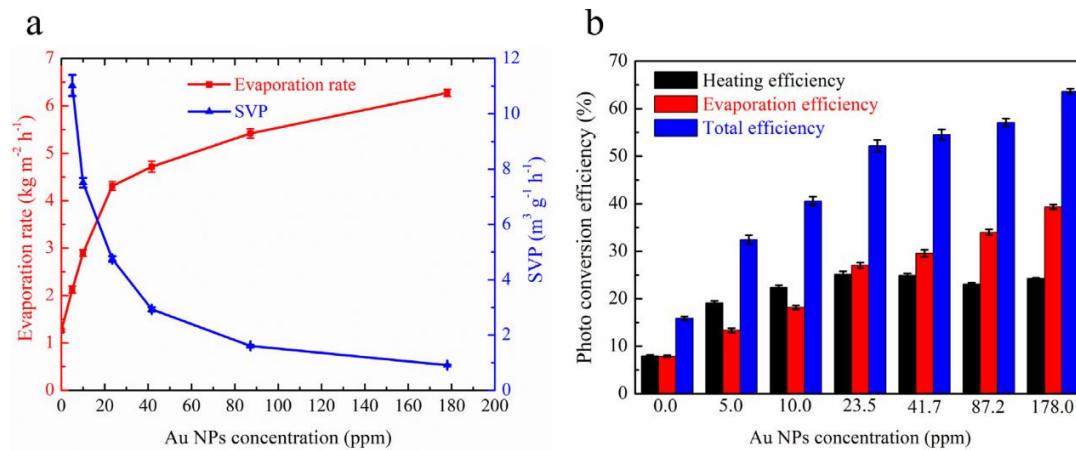


Figure 20. (a) Evaporation rate and specific vapor productivity (SVP) change as a function of Au nanoparticle concentration; (b) heating efficiency, evaporation efficiency, and total efficiency during solar steam generation [44]; 2017, Elsevier.

The above-mentioned studies reported that nanomaterials can enhance the photothermal energy conversion performance by improving the photothermal energy conversion characteristics of working fluids. Moreover, some studies even suggested that further improvement in the photo-thermal energy conversion of nanofluid is possible by applying additional forces such as an external magnetic field. The next section introduces and discusses representative studies on the applications of the photothermal energy conversion characteristics of nanofluids. Photothermal energy conversion processes are usually applied in two main applications: solar thermal collectors and solar-driven steam generators or evaporators.

5. Application of Photothermal Energy Conversion Technique Using Nanofluids

5.1. Solar Thermal Collectors

One of the main engineering applications that uses the photothermal energy conversion process of nanofluids is the solar thermal collector. Solar collectors are generally used for domestic water heating, space heating, and industrial low-temperature applications, and the overall efficiency of the solar thermal collector is approximately 70% [69]. Table 3 [70] classifies solar thermal collectors according to their operating temperature range into low-, middle-, and high-temperature ranges. In addition, depending on the manufactured structure, the solar thermal collector can be classified into flat-plate, evacuated-tube, heat-pipe, and parabolic solar collectors. Table 4 [71] lists representative application areas and the types of solar collectors that can be used for each area. However, because these existing solar collectors collect heat through several steps, such as heat absorption and the transfer of the working fluid, there are various losses that decrease the efficiency of these solar collectors. Hence, there is an urgent need to develop a direct absorption solar collector (DASC) that eliminates the heat transfer process and absorbs heat directly from light. To develop a high-efficiency DASC, the photothermal energy conversion efficiency of the working fluid is the most important factor.

Table 3. Classification of solar collectors according to temperature level [70]; 2017, WorldSciNet.

Item	Low Temperature		Middle Temperature	High Temperature
Temperature range, °C	<60	<100	<300	>300
Type	Flat-plate collector	Evacuated-tube collector	PTC, CPC	Parabolic collector

Table 4. Solar thermal collectors for different applications [71]; 2009, Elsevier.

Application	Type	Circulation
Solar water heating	Flat-plate collector	Natural/Forced
	Evacuated tube	
Space heating and cooling	Compound parabolic collector	Forced
	Flat-plate collector	
	Evacuated tube	
Solar refrigeration	Compound parabolic collector	Forced
	Flat-plate collector	
	Evacuated tube	
Industrial process heat	Compound parabolic collector	Forced
	Flat-plate collector	
	Evacuated tube	
	Compound parabolic collector	
Solar desalination	Parabolic trough collector	Natural/Forced
	Linear Fresnel collector	
	Flat-plate collector	
	Evacuated tube	
	Compound parabolic collector	
Solar thermal power	Parabolic trough collector	Forced
	Heliostat field collector	
	Compound parabolic collector	
	Parabolic dish collector	
	Linear Fresnel collector	
Simultaneous generation of electricity and heat	PV/T collector	Forced

To estimate the thermal efficiency of solar collectors, Equation (6) [70] can be used:

$$\eta = \frac{Q_u}{A_c G} = \frac{m C_p (T_o - T_i)}{A_c G} \quad (6)$$

where Q_u , C_p , and m are the useful heat gain, specific heat, and mass flow rate of the working fluid, respectively; T_o and T_i are the outlet and inlet temperatures of the working fluid, respectively; and A_c is the surface area of the solar collector. In addition, Q_u can be calculated using Equation (7):

$$Q_u = m C_p (T_o - T_i) = A_c F_R [G(\tau\alpha) - U_L(T_i - T_a)] \quad (7)$$

where F_R and G are the heat removal factor and incident solar irradiation, respectively; $\tau\alpha$ and U_L are the absorption transmittance product and overall loss coefficient of the solar collector, respectively; and T_a is the ambient air temperature.

Tyagi et al. [72] theoretically investigated the performance of DASC using Al_2O_3 nanofluid (0.1vol% to 5vol%). Kim et al. [73] theoretically studied and compared the efficiency of a U-tube solar thermal collector by applying different types of nanofluids. The maximum efficiency enhancement was observed for a U-tube solar thermal collector using 0.2vol% MWCNT nanofluid, followed by CuO, Al_2O_3 , TiO_2 , and SiO_2 nanofluids at a concentration of 3vol%. The overall efficiency of the solar thermal collector increased by 8% when the concentration of the Al_2O_3 nanofluid increased from 0.8vol% to 1.6vol%. Furthermore, they stressed that the effect of nanoparticle size on the efficiency enhancement is marginal. Saffarian et al. [74] numerically studied the convective heat transfer enhancement of a flat-plate solar thermal collector with different flow paths by using various types of nanofluids. The highest heat transfer enhancement was observed for 4vol% CuO/water nanofluid, amongst other working fluids such as Al_2O_3 /water and water. Hussein et al. [75] experimentally studied a flat-plate solar thermal collector using water-based covalent functionalized MWCNT and covalently functionalized graphene nanoplatelets (CF-GNP) with a hexagonal boron nitride (hBN) nanofluid. The overall performance of the solar thermal collector increased with increasing nanofluid concentration. Furthermore, the performance of the flat-plate solar thermal collectors was enhanced by up to 85% at 0.1 wt% CF-GNP h-BN nanofluid, which is 20% higher than the performance enhancement for DI

water. Tong et al. [76] comprehensively investigated DI-water-based Al_2O_3 , CuO, MWCNT, and Fe_3O_4 nanofluids in a flat-plate solar collector. All of the nanofluid cases exhibited significantly higher collector efficiencies than the DI-water case. According to Figure 21, a maximum overall efficiency of 87% was observed for 0.005vol% MWCNT nanofluid. Kang et al. [77] studied an evacuated solar thermal collector using CuO nanoparticles with different diameters. Their results indicate that smaller CuO nanoparticles resulted in superior thermal efficiency in the evacuated solar thermal collector. Kim et al. [78] experimentally examined the effect of the size and concentration of Al_2O_3 nanoparticles on the performance of a U-tube solar collector. They reported that the thermal conductivity of the Al_2O_3 nanofluid increased as the size of the nanoparticles decreased. Figure 22 shows the variation in the efficiency of their U-tube solar collector. The efficiency of the U-tube solar collector increased as the size of the Al_2O_3 nanoparticles decreased under the experimental conditions. In addition, Tong et al. [79] investigated the energy efficiency, entropy generation, exergy destruction, and exergy efficiency of flat-plate solar collectors using water-based Al_2O_3 and CuO nanofluids. The lowest entropy generation and highest efficiency were observed when Al_2O_3 nanofluid was used in the flat-plate solar thermal collector in comparison with CuO nanofluid and DI water. Yurddas et al. [80] numerically and experimentally optimized the technical and geometric values of an open-ended evacuated solar thermal collector with MWCNT, TiO_2 , SiO_2 , and Cu nanofluids while considering various parameters. The results indicated that the thermal efficiency of the solar thermal collector increased with the length and diameter of the vacuum tube. Among the different nanofluids, the Cu- H_2O nanofluid exhibited the best results, with a 14.09% enhancement in heat transfer.

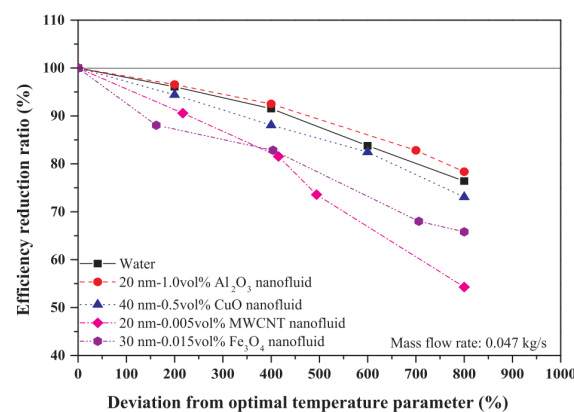


Figure 21. Reduction in the photothermal energy conversion efficiency of nanofluids according to the deviation from the optimal temperature [76]; 2020, Elsevier.

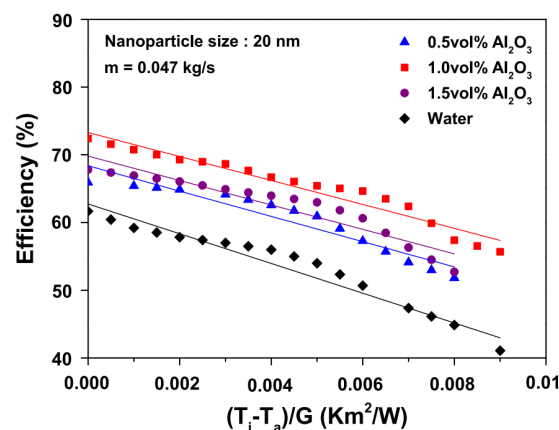


Figure 22. Variation of the efficiency of a U-tube solar collector as a function of nanoparticle size (nanofluid concentration: 1vol%, $m = 0.047$ kg/s) [78]; 2017, Elsevier.

To compensate for the high cost and low efficiency of PV modules, hybrid PV thermal solar collector (PV/T) systems have been intensively studied in recent years. The significance of the PV/T system is that it can simultaneously produce electric and thermal energy. Razali et al. [81] summarized representative studies on the analysis of PV/T systems in Table 5 [82–86]. As summarized in the table, metal-oxide nanoparticles with small diameters tended to be used in PV/T hybrid systems.

Table 5. Summary of performance of nanofluid-based PV/T systems [81]; 2019, IAES.

Ref.	Nanofluid	Particle Size, nm	Concentration	Results
[82]	SiO ₂	11–14	1, 3 wt%	For 1wt% and 3wt%, the energy conversion efficiency increased by up to 3.6% and 7.9%.
[83]	Fe ₃ O ₄	-	1, 3 wt%	The total exergy increased on adding the nanofluid; for 3 wt%, the overall efficiency improved by 45%; when an alternating magnetic field (50 Hz) is applied, the overall efficiency increased by up to 50%. The transmittance of nanofluids decreases as the mass fraction and film thickness increase; the overall efficiency of the PV/T system with a 2-mm-thick liquid layer is greater than 60%.
[84]	MgO	10	0.02, 0.006, 0.1	The transmittance of a 2vol% nanofluid with a particle size of 5 nm can be as high as 97%, which is very close to that of pure water; nanofluids with smaller nanoparticles show a higher thermal conductivity than those with larger nanoparticles.
[85]	SiO ₂	5–50	2vol%	A volume fraction of 0.0011% is required to achieve optimum filters.
[86]	Au, SiO ₂ , Al, Ag	20–50	0.01vol%	

Numerous studies have shown that the efficiency of the solar thermal collector can be increased when various nanofluids are used as the working fluid. In addition, the thermal and overall efficiency of the various solar thermal collectors depend on the type of nanofluid and the properties of nanoparticles such as size and shape. Moreover, the dispersion stability of nanofluids is a critical factor in maintaining the high efficiency of solar collectors using nanofluids.

5.2. Solar-Driven Steam Generators

One of the cheapest ways to generate steam is to use solar energy; however, solar steam generation has a lower energy efficiency than other technologies. Steam generation can be combined with other processes for various engineering applications such as water distillation or extraction [87], hydrogen production [88], separation of mixed solvents [89], mixed solvent separation [90], and even food processing [91]. To efficiently use solar energy, the absorbing working fluid should have full-spectrum broadband solar absorption. Therefore, DI water alone is not suitable as the working fluid for steam generation systems. Significant attempts have been made to use materials such as volumetric absorbers, gas-particle suspensions, and molten salts [92] as the working fluid.

According to Dao et al. [93], by widening the solar absorption spectrum of working fluids, nanoparticles showed a high potential to enhance the efficiency of solar steam generation, as shown in Figure 23. Generally, solar steam generation technologies are categorized into two groups: surface absorption [94–96] and volumetric absorption [66–70] solar steam generation. In Figure 24, Wang et al. [90,97] presented a bio-inspired evaporation film from localized evaporative biological processes such as sweating and transpiration. Furthermore, to control the local temperature of the evaporative surface, plasmonic heating was applied. Figure 25 shows an infrared image of a sample beaker with a plasmonic film at the top of the sample. Figure 25a clearly shows that the sample exhibited a uniform temperature distribution throughout; however, after laser irradiation, most of

the absorbed energy was focused on the plasmonic surface, leading to high steam generation in the sample in Figure 25e. Huang et al. [94] improved the evaporation using a C-TiO₂ solar absorber system, which is shown in Figure 26, and their experimental results are shown in Figure 27. They reported that the evaporation mass change increased with an increase in the evaporation area of the C-TiO₂ absorber under irradiation at 1 kW/m².

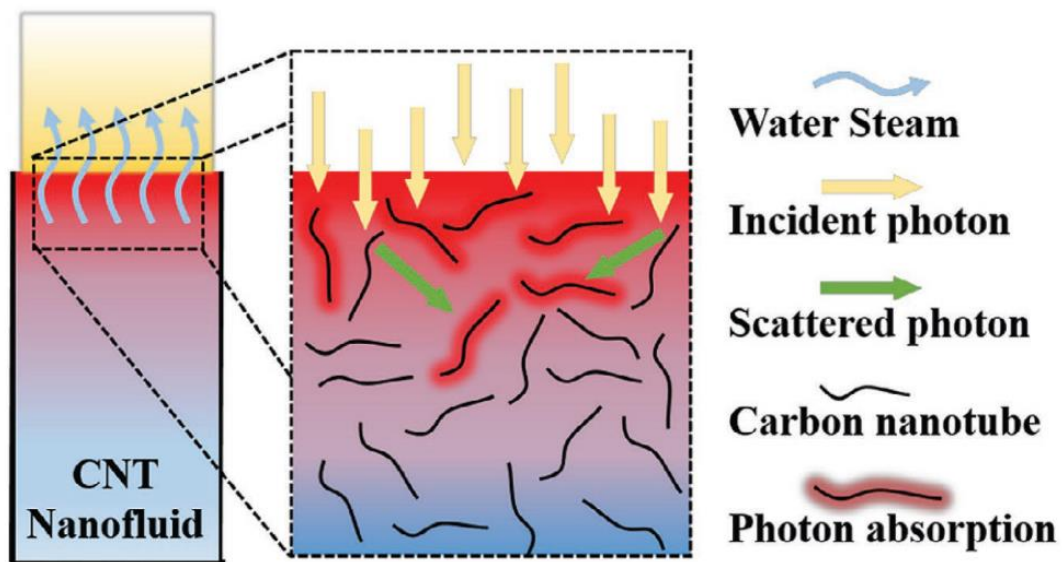


Figure 23. Schematic of the localized solar heating and steam generation mechanism [93]; 2018, Wiley.

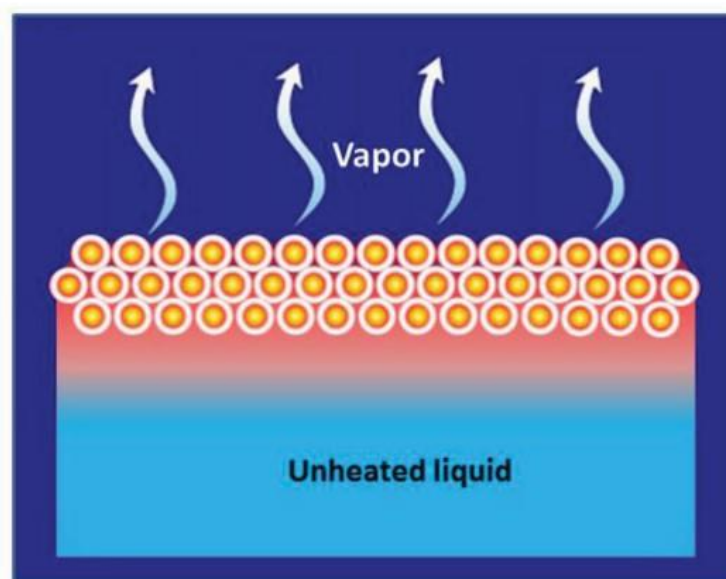


Figure 24. Schematic illustration of liquid plasmonic evaporation mechanism assisted by floating surface absorber [90]; 2014, Wiley.

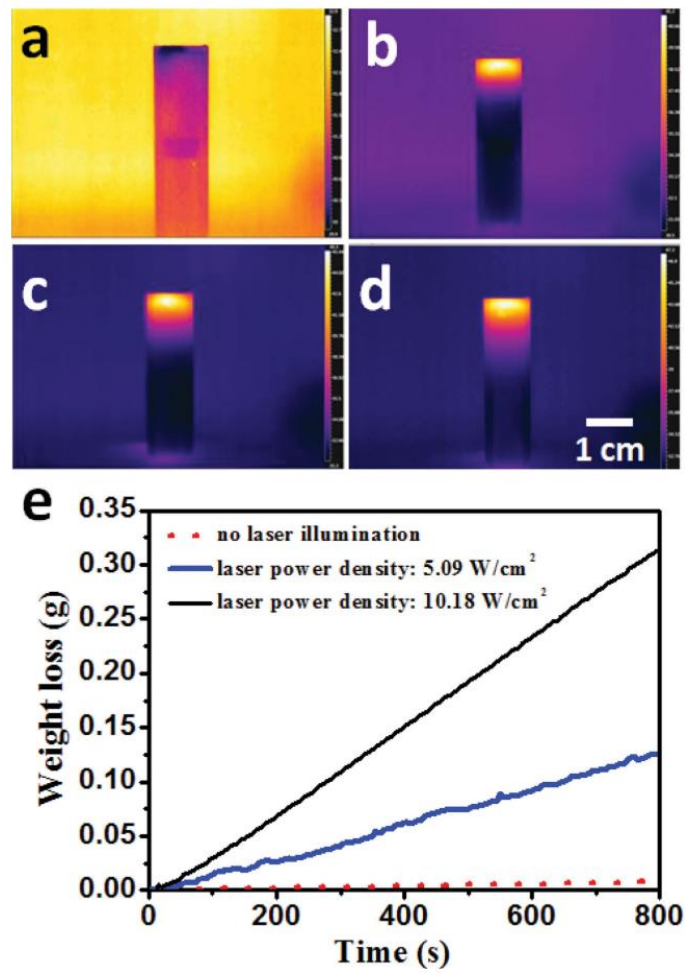


Figure 25. (a–d) IR images of gold nanofluid evaporation under irradiation laser illumination, and (e) evaporation rate under different laser power densities [90]; 2014, Wiley.

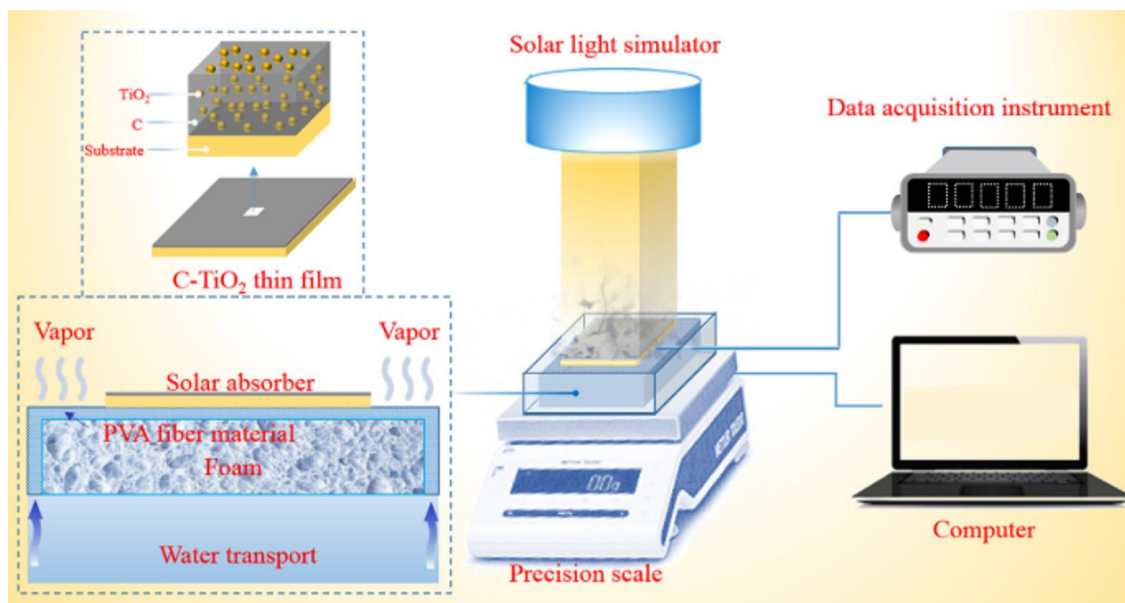


Figure 26. Experimental schematic of the C-TiO₂ solar water evaporator [94]; 2019, Elsevier.

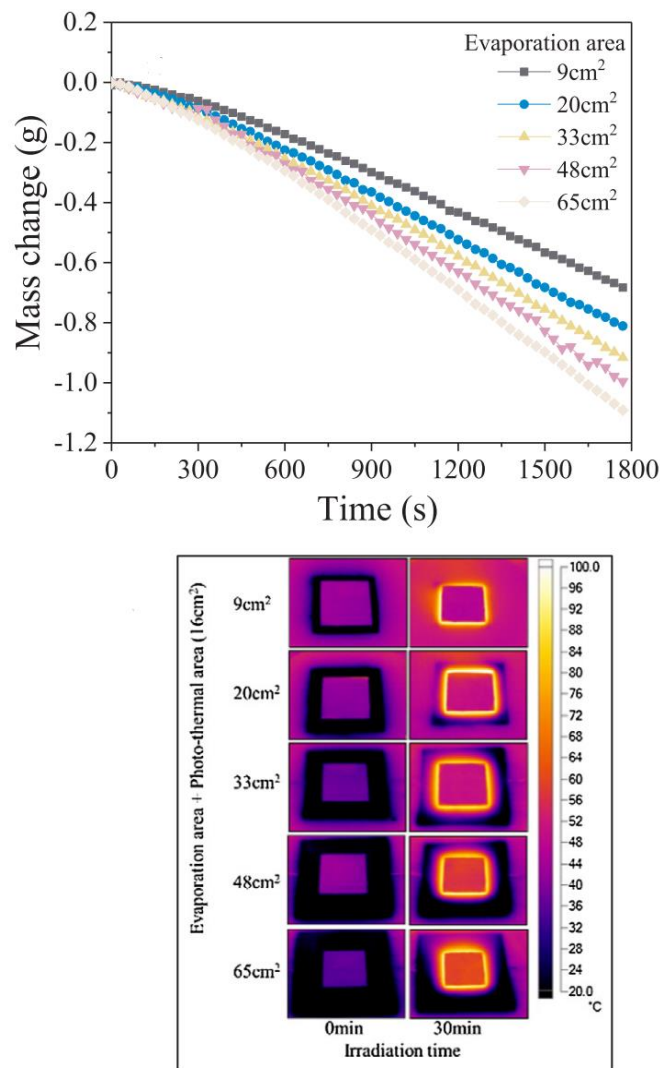


Figure 27. Evaporation mass change and temperature distribution in different evaporation regions [94]; 2019, Elsevier.

Sajadi et al. [91] proposed flexible artificially networked structured alternative surfaces for solar steam generation. These surfaces are differently manufactured artificially networked 3D porous polymers with graphite coatings. Figure 28 shows a schematic of the flexible artificially networked structure for ambient/high-pressure solar steam generation. They reported that these structures performed significantly better in heat localization than the structures used in previous studies and led to a higher performance in solar-driven steam generation. In these structures, the generated steam was in a temperature range of 100–156 °C and a pressure range of 100–525 kPa. Wang et al. [95] reported that when the surface temperature of pure water increased to 33.2 °C, that of beakers with graphene oxide (GO) and reduced GO (rGO) surface absorbers increased to 52.1 °C and 46.8 °C, respectively. IR images of these beakers are shown in Figure 29. Fu et al. [98] investigated a volumetric solar steam generator that uses Au and GO nanoparticles. The evaporation rate was significantly increased when nanofluids were used instead of pure water. A maximum evaporation mass change rate of 0.33 kgm⁻²min⁻¹ was observed at a GO-Au concentration of 15.6 wt%, and the efficiency of steam generation was 59.2%, which was 2.6% higher than that of pure water.

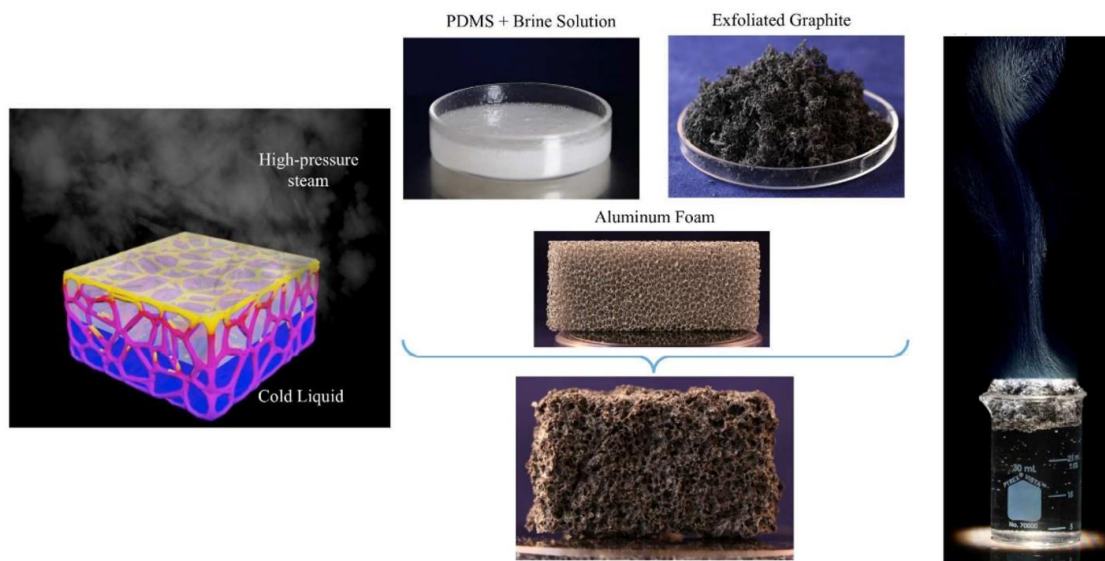


Figure 28. Schematics of flexible artificially networker floating surface absorbing evaporators [91]; 2016, RSC.

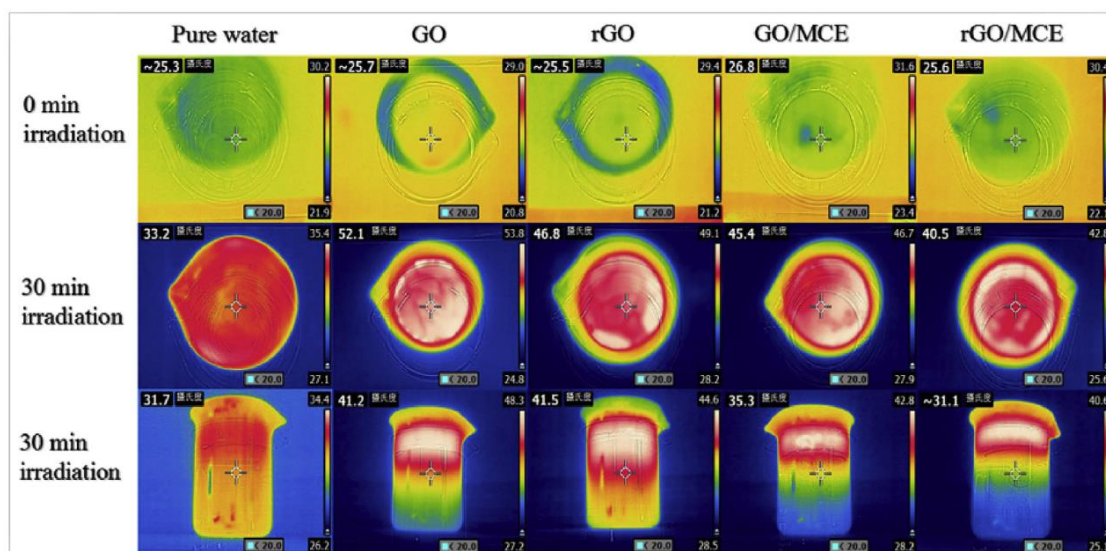


Figure 29. Surface temperatures of bulk water in different samples before and after solar illumination, and the whole water temperature distribution after illumination (IR camera) [95]; 2017, Elsevier.

Liu et al. [99] studied the volumetric solar-driven steam generation of rGO nanofluid. According to the IR images of water and rGO nanofluids shown in Figure 30, after 60 min of irradiation, water has a more uniform temperature distribution than the rGO nanofluid. In the case of the rGO nanofluid, most of the absorbed energy was concentrated at the top layer of the sample, which significantly enhanced the steam generation in the nanofluid. Zeiny et al. [100] examined the solar evaporation of plasmonic Au nanofluids at different concentrations. As Figure 31 clearly shows, the temperature is distributed non-uniformly in a sample beaker owing to the additional nanoparticles in water. Moreover, the thickness of the hot thin layer of nanofluid in the beaker decreased with an increase in the Au nanofluid concentration, resulting in highly efficient evaporation.

In summary, each experiment exhibited the same result (localized heating), although volumetric and surface evaporation methods used a different process to enhance the solar-driven steam generation. From some studies based on the volumetric absorption method, it can be concluded that waves are scattered in the top layer of the sample owing to the interaction between nanoparticles and light, causing localized heating in a nanofluid. However, in the case of the surface absorption method, a plasmonic sheet and foam with high light absorbance emit solar energy to the top of the sample, causing localized heating in the sample.

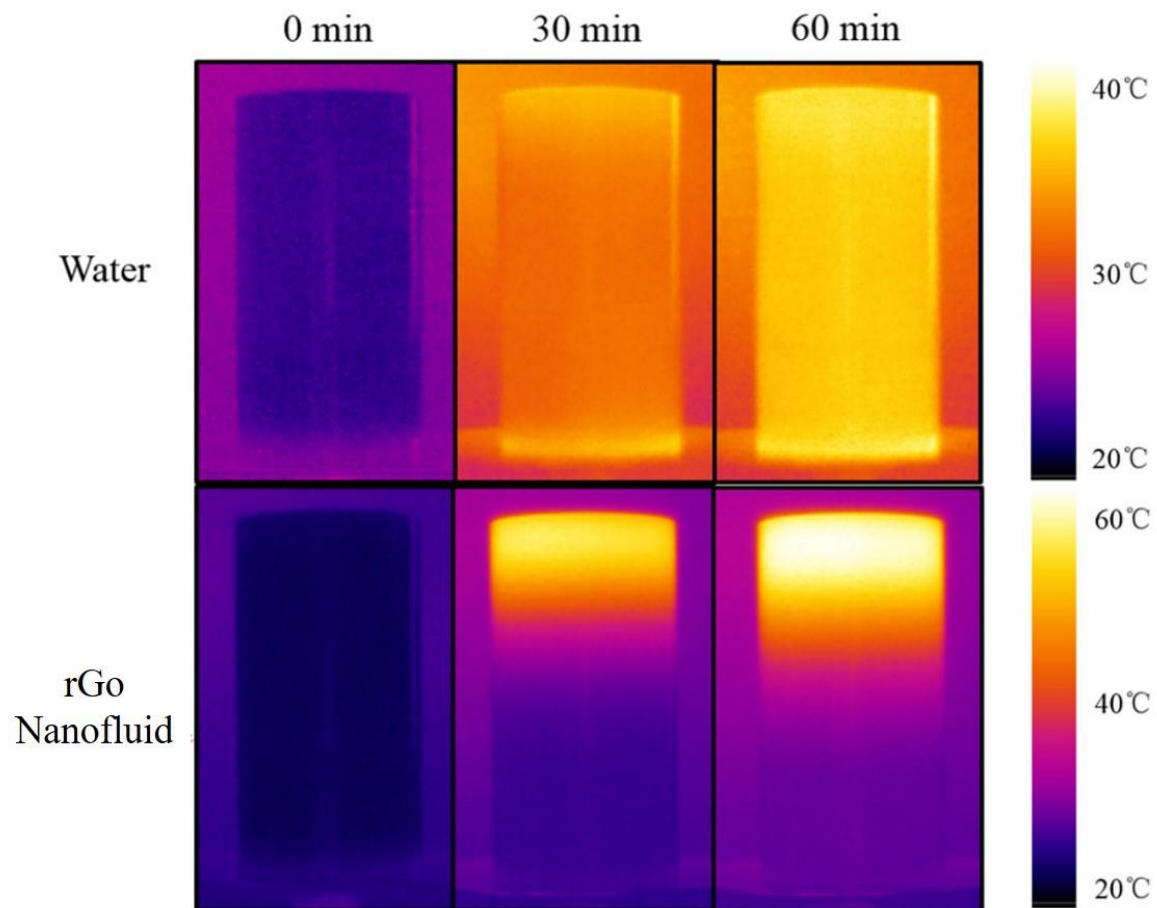


Figure 30. IR thermal images of water and rGO nanofluid at different times [99]; 2018, Elsevier.

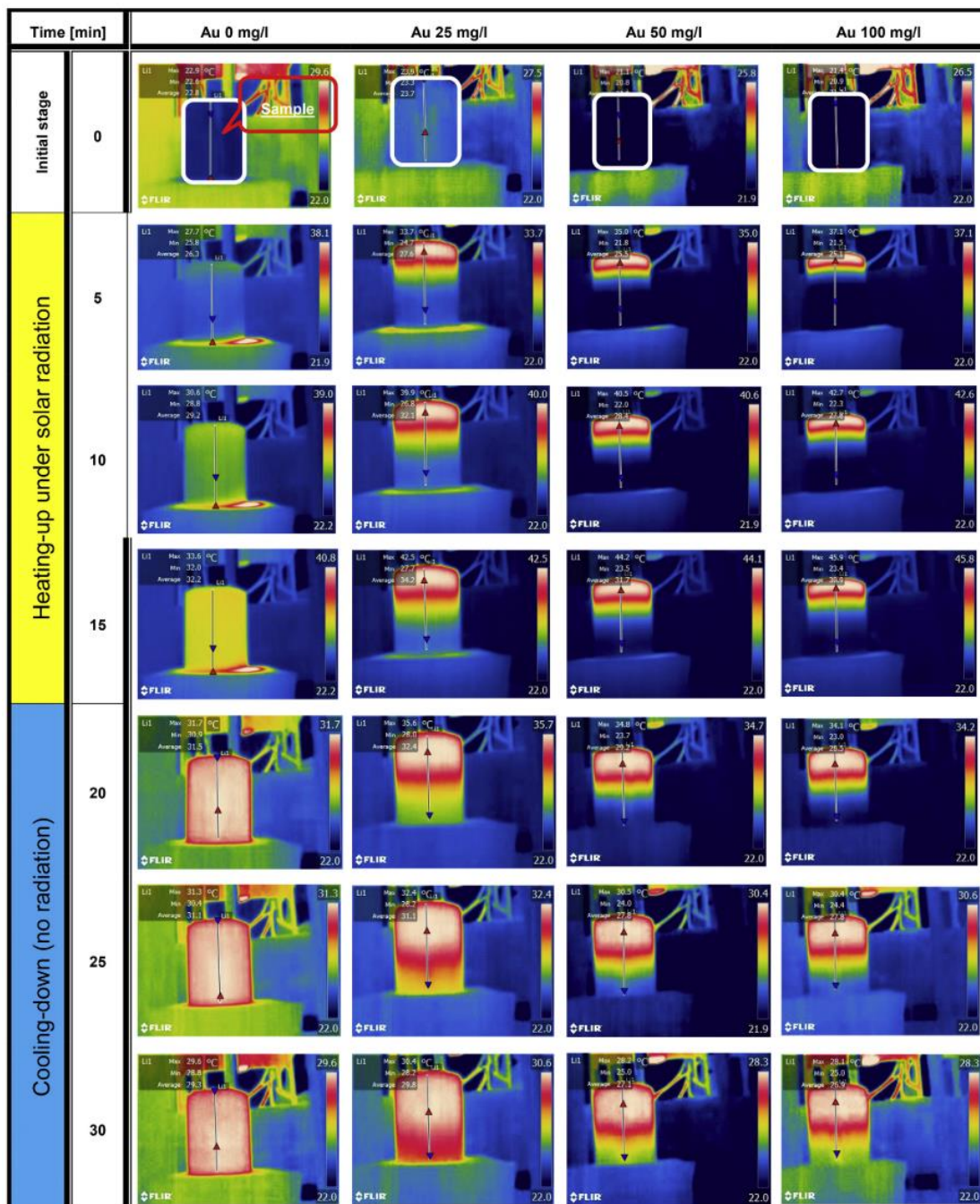


Figure 31. Heating (under radiation) and cooling (no radiation) process of gold nanofluid with different nanofluid concentrations [100]; 2018, Elsevier.

6. Concluding Remarks and Directions for Future Research

This article reviewed the state of research on the photothermal energy conversion performance of various nanofluids and their applications, with a focus on the two sub-properties that affect the photothermal energy conversion of working fluids: preparation and optical characteristics of nanofluids. In addition, the current status of the photothermal energy conversion performance of existing nanofluids has been extensively discussed.

Numerous studies on the photothermal energy conversion performance of nanofluids have been discussed, and they employed various nanostructures such as carbon materials and metal oxides. Previous studies have shown that nanomaterials can enhance the photothermal energy conversion

performance by improving the photothermal energy conversion characteristics of working fluids. Moreover, some studies even suggest that the photothermal energy conversion of nanofluids can be further improved by applying additional forces such as an external magnetic field. In addition, the sub-properties indicate that the dispersion stability of nanofluids can significantly affect their photothermal energy conversion process. Moreover, most of the performance enhancements in photothermal energy conversion were caused by improvements in the optical characteristic, such as the broadening of the solar absorption spectrum. Among the nanofluids, carbon materials such as MWCNT and GO nanofluids dominantly exhibited photo-thermal energy conversion enhancements. The photothermal energy conversion process is mainly used in solar thermal collectors and solar-driven steam generators.

According to the outcomes of this literature survey, it has been taken attention that most of these investigations have focused on the effect of the concentration and types of nanofluid on photothermal energy conversion efficiency. However, there are many other effects could not be examined such as the size, shape, and accessibility of nanoparticles. Even though plasmonic nanoparticles such as Au and Ag have a high potential to enhance photothermal energy conversion efficiency, accessibility, and synthesis of these nanoparticles in the industrial application are another major challenge for researchers. In addition, some of the plasmonic and other nanoparticles as mentioned in previous studies are rare earth elements; thus, these are not economically affordable in the market. To develop a high efficiency sustainable energy harvesting system, such rare and expensive nanoparticles should be replaced with other new or conventional nanoparticles. In addition, the previous investigations related to the nanofluid application in solar thermal collectors mentioned that the highest efficiency was mostly observed at the highest concentration of nanofluid in their experimental ranges. However, the concentration of the nanofluid in the system should be seriously reconsidered because an increment in the nanofluid concentration can bring the increase of viscosity of working fluid in the system, which always causes the increase in pumping power consumption. Lastly, the optical nanofluid concentration for each nanofluid and various systems is also investigated preciously under wide operating conditions. For some future studies, water extraction in industrial and seawater distillation applications for clean drinking water can be essential ones. In addition, there is a vast idle space for new studies such as solar thermoelectric cells, absorption cooling and heating transformers that powered by the low heat input such as solar energy, and solar powered seasonal thermal energy storage, etc.

Author Contributions: Conceptualization, H.C. and T.B.; methodology, J.H.; validation, H.C., T.B., and J.H.; formal analysis, E.K. and J.H.; investigation, E.K. and T.B.; resources, H.C.; writing—original draft preparation, T.B. and E.K.; writing—review and editing, H.C. and J.H.; visualization, T.B. and E.K.; supervision, H.C. All authors have read and agreed to the published version of the manuscript.

Funding: This research was supported by the Basic Science Research Program through the National Research Foundation of Korea (NRF) funded by the Ministry of Science, ICT & Future Planning (NRF-2020R1A2C2008248) and Human Resources Program in Energy Technology of the Korea Institute of Energy Technology Evaluation and Planning (KETEP), granted financial resources from the Ministry of Trade, Industry & Energy, Republic of Korea(No. 20194030202410).

Conflicts of Interest: The authors declare no conflict of interest. The funders had no role in the design of the study; in the collection, analyses, or interpretation of data; in the writing of the manuscript, or in the decision to publish the results.

References

1. Ghezloun, A.; Saidane, A.; Oucher, N.; Chergui, S. The Post-Kyoto. *Energy Procedia* **2013**, *36*, 1–8. [[CrossRef](#)]
2. World Energy Outlook. 2018. Available online: www.iea.org/weo2018 (accessed on 10 August 2020).
3. Gao, M.; Zhu, L.; Peh, C.K.N.; Ho, G.W. Solar absorber material and system designs for photothermal water vaporization towards clean water and energy production. *Energy Environ. Sci.* **2019**, *12*, 841–864. [[CrossRef](#)]
4. Ghalandari, M.; Maleki, A.; Haghighi, A.; Shadloo, M.S.; Nazari, M.A.; Tlili, I. Applications of nanofluids containing carbon nanotubes in solar energy systems: A review. *J. Mol. Liq.* **2020**, *313*, 113476. [[CrossRef](#)]

5. Dubey, S.; Sarvaiya, J.N.; Seshadri, B. Temperature Dependent Photovoltaic (PV) Efficiency and Its Effect on PV Production in the World—A Review. *Energy Procedia* **2013**, *33*, 311–321. [[CrossRef](#)]
6. Weinberger, H. The physics of the solar pond. *Sol. Energy* **1964**, *8*, 45–56. [[CrossRef](#)]
7. Anagnostopoulos, A.; Sebastia-Saez, D.; Campbell, A.N.; Arellano-Garcia, H. Finite element modelling of the thermal performance of salinity gradient solar ponds. *Energy* **2020**, *203*, 117861. [[CrossRef](#)]
8. Yu, F.; Chen, Y.; Liang, X.; Xu, J.; Lee, C.; Liang, Q.; Tao, P.; Deng, T. Dispersion stability of thermal nanofluids. *Prog. Nat. Sci.* **2017**, *27*, 531–542. [[CrossRef](#)]
9. Ilyas, S.U.; Pendyala, R.; Narahari, M. Preparation, Sedimentation, and Agglomeration of Nanofluids. *Chem. Eng. Technol.* **2014**, *37*, 2011–2021. [[CrossRef](#)]
10. Taha-Tijerina, J.J. Thermal transport and challenges on nanofluids performance. In *Microfluidics and Nanofluidics*; IntechOpen: London, UK, 2018. [[CrossRef](#)]
11. Ilyas, S.U.; Pendyala, R.; Narahari, M. Stability of Nanofluids. *Aerospace Alloy.* **2017**, 1–31. [[CrossRef](#)]
12. Bhalla, V.; Khullar, V.; Tyagi, H. Experimental investigation of photo-thermal analysis of blended nanoparticles ($\text{Al}_2\text{O}_3/\text{Co}_3\text{O}_4$) for direct absorption solar thermal collector. *Renew. Energy* **2018**, *123*, 616–626. [[CrossRef](#)]
13. Shi, L.; Wang, X.; Hu, Y.; He, Y. Investigation of photocatalytic activity through photo-thermal heating enabled by $\text{Fe}_3\text{O}_4/\text{TiO}_2$ composite under magnetic field. *Sol. Energy* **2020**, *196*, 505–512. [[CrossRef](#)]
14. Zeng, J.; Xuan, Y. Enhanced solar thermal conversion and thermal conduction of MWCNT-SiO₂/Ag binary nanofluids. *Appl. Energy* **2018**, *212*, 809–819. [[CrossRef](#)]
15. Fang, J.; Zhang, P.; Chang, H.; Wang, X. Hydrothermal synthesis of nanostructured CuS for broadband efficient optical absorption and high-performance photo-thermal conversion. *Sol. Energy Mater. Sol. Cells* **2018**, *185*, 456–463. [[CrossRef](#)]
16. Zhao, R.; Xu, J.; Tao, P.; Shi, F.; Yu, F.; Zeng, X.; Song, C.; Wu, J.; Shang, W.; Deng, T. Clean water generation with switchable dispersion of multifunctional Fe_3O_4 -reduced graphene oxide particles. *Prog. Nat. Sci.* **2018**, *28*, 422–429. [[CrossRef](#)]
17. Liu, Z.; Yan, Y.; Fu, R.; Alsaady, M. Enhancement of solar energy collection with magnetic nanofluids. *Therm. Sci. Eng. Prog.* **2018**, *8*, 130–135. [[CrossRef](#)]
18. Amjad, M.; Jin, H.; Du, X.; Wen, D. Experimental photothermal performance of nanofluids under concentrated solar flux. *Sol. Energy Mater. Sol. Cells* **2018**, *182*, 255–262. [[CrossRef](#)]
19. Zeiny, A.; Jin, H.; Bai, L.; Lin, G.; Wen, D. A comparative study of direct absorption nanofluids for solar thermal applications. *Sol. Energy* **2018**, *161*, 74–82. [[CrossRef](#)]
20. Yao, G.; Xu, J.; Liu, G. Solar steam generation enabled by bubbly flow nanofluids. *Sol. Energy Mater. Sol. Cells* **2020**, *206*, 110292. [[CrossRef](#)]
21. Ulset, E.T.; Kosinski, P.; Zbednova, Y.; Zhdaneev, O.V.; Struchalin, P.G.; Balakin, B.V. Photothermal boiling in aqueous nanofluids. *Nano Energy* **2018**, *50*, 339–346. [[CrossRef](#)]
22. Wang, F.; Ling, Z.; Fang, X.; Zhang, Z. Optimization on the photo-thermal conversion performance of graphite nanoplatelets decorated phase change material emulsions. *Sol. Energy Mater. Sol. Cells* **2018**, *186*, 340–348. [[CrossRef](#)]
23. Beicker, C.L.; Amjad, M.; Filho, E.P.B.; Wen, D. Experimental study of photothermal conversion using gold/water and MWCNT/water nanofluids. *Sol. Energy Mater. Sol. Cells* **2018**, *188*, 51–65. [[CrossRef](#)]
24. Mehrali, M.; Ghatkesar, M.K.; Pecnik, R. Full-spectrum volumetric solar thermal conversion via graphene/silver hybrid plasmonic nanofluids. *Appl. Energy* **2018**, *224*, 103–115. [[CrossRef](#)]
25. Chen, M.; He, Y.; Ye, Q.; Zhang, Z.; Hu, Y. Solar thermal conversion and thermal energy storage of CuO/Paraffin phase change composites. *Int. J. Heat Mass Transf.* **2019**, *130*, 1133–1140. [[CrossRef](#)]
26. Wang, L.; Zhu, G.; Wang, M.; Yu, W.; Zeng, J.; Yu, X.; Xie, H.; Li, Q. Dual plasmonic Au/TiN nanofluids for efficient solar photothermal conversion. *Sol. Energy* **2019**, *184*, 240–248. [[CrossRef](#)]
27. Qu, J.; Zhang, R.; Wang, Z.; Wang, Q. Photo-thermal conversion properties of hybrid CuO-MWCNT/H₂O nanofluids for direct solar thermal energy harvest. *Appl. Therm. Eng.* **2019**, *147*, 390–398. [[CrossRef](#)]
28. Mishra, A.K.; Lahiri, B.; Philip, J. Superior thermal conductivity and photo-thermal conversion efficiency of carbon black loaded organic phase change material. *J. Mol. Liq.* **2019**, *285*, 640–657. [[CrossRef](#)]
29. Hazra, S.; Ghosh, S.; Nandi, T. Photo-thermal conversion characteristics of carbon black-ethylene glycol nanofluids for applications in direct absorption solar collectors. *Appl. Therm. Eng.* **2019**, *163*, 114402. [[CrossRef](#)]

30. Zhu, G.; Wang, L.; Bing, N.; Xie, H.; Yu, W. Enhancement of photothermal conversion performance using nanofluids based on bimetallic Ag-Au alloys in nitrogen-doped graphitic polyhedrons. *Energy* **2019**, *183*, 747–755. [[CrossRef](#)]
31. Wang, D.; Jia, Y.; He, Y.; Wang, L.; Xie, H.; Yu, W. Photothermal efficiency enhancement of a nanofluid-based direct absorption solar collector utilizing magnetic nano-rotor. *Energy Convers. Manag.* **2019**, *199*, 111996. [[CrossRef](#)]
32. Nourafkan, E.; Asachi, M.; Jin, H.; Wen, D.; Ahmed, W. Stability and photo-thermal conversion performance of binary nanofluids for solar absorption refrigeration systems. *Renew. Energy* **2019**, *140*, 264–273. [[CrossRef](#)]
33. Walshe, J.; Amarandei, G.; Ahmed, H.; McCormack, S.; Doran, J. Development of poly-vinyl alcohol stabilized silver nanofluids for solar thermal applications. *Sol. Energy Mater. Sol. Cells* **2019**, *201*, 110085. [[CrossRef](#)]
34. Jin, H.; Lin, G.; Bai, L.; Amjad, M.; Filho, E.P.B.; Wen, D. Photothermal conversion efficiency of nanofluids: An experimental and numerical study. *Sol. Energy* **2016**, *139*, 278–289. [[CrossRef](#)]
35. Jin, X.; Lin, G.; Zeiny, A.; Jin, H.; Bai, L.; Wen, D. Solar photothermal conversion characteristics of hybrid nanofluids: An experimental and numerical study. *Renew. Energy* **2019**, *141*, 937–949. [[CrossRef](#)]
36. Hong, Z.; Pei, J.; Wang, Y.; Cao, B.; Mao, M.; Liu, H.; Jiang, H.; An, Q.; Liu, X.; Hu, X. Characteristics of the direct absorption solar collectors based on reduced graphene oxide nanofluids in solar steam evaporation. *Energy Convers. Manag.* **2019**, *199*, 112019. [[CrossRef](#)]
37. Struchalin, P.; Thon, H.; Kuzmenkov, D.; Kutsenko, K.; Kosinski, P.; Balakin, B. Solar steam generation enabled by iron oxide nanoparticles: Prototype experiments and theoretical model. *Int. J. Heat Mass Transf.* **2020**, *158*, 119987. [[CrossRef](#)]
38. Wang, T.; Tang, G.; Du, M. Photothermal conversion enhancement of triangular nanosheets for solar energy harvest. *Appl. Therm. Eng.* **2020**, *173*, 115182. [[CrossRef](#)]
39. Tong, Y.; Boldoo, T.; Ham, J.; Cho, H. Improvement of photo-thermal energy conversion performance of MWCNT/Fe₃O₄ hybrid nanofluid compared to Fe₃O₄ nanofluid. *Energy* **2020**, *196*, 117086. [[CrossRef](#)]
40. Guo, C.; Liu, C.; Jiao, S.; Wang, R.; Rao, Z. Introducing optical fiber as internal light source into direct absorption solar collector for enhancing photo-thermal conversion performance of MWCNT-H₂O nanofluids. *Appl. Therm. Eng.* **2020**, *173*, 115207. [[CrossRef](#)]
41. Shin, Y.; Ham, J.; Boldoo, T.; Cho, H. Magnetic effect on the enhancement of photo-thermal energy conversion efficiency of MWCNT/Fe₃O₄ hybrid nanofluid. *Sol. Energy Mater. Sol. Cells* **2020**, *215*, 110635. [[CrossRef](#)]
42. Vijayanandan, A.S.; Valappil, R.S.K.; Balakrishnan, R.M. Evaluation of photothermal properties for absorption of solar energy by Co₃O₄ nanofluids synthesized using endophytic fungus *Aspergillus nidulans*. *Sustain. Energy Technol. Assess.* **2020**, *37*, 100598. [[CrossRef](#)]
43. Zhang, H.; Chen, H.-J.; Du, X.; Wen, D. Photothermal conversion characteristics of gold nanoparticle dispersions. *Sol. Energy* **2014**, *100*, 141–147. [[CrossRef](#)]
44. Wang, X.; He, Y.; Liu, X.; Shi, L.; Zhu, J. Investigation of photothermal heating enabled by plasmonic nanofluids for direct solar steam generation. *Sol. Energy* **2017**, *157*, 35–46. [[CrossRef](#)]
45. Amjad, M.; Raza, G.; Xin, Y.; Pervaiz, S.; Xu, J.; Du, X.; Wen, D. Volumetric solar heating and steam generation via gold nanofluids. *Appl. Energy* **2017**, *206*, 393–400. [[CrossRef](#)]
46. Hogan, N.J.; Urban, A.S.; Ayala-Orozco, C.; Pimpinelli, A.; Nordlander, P.; Halas, N.J. Nanoparticles Heat through Light Localization. *Nano Lett.* **2014**, *14*, 4640–4645. [[CrossRef](#)] [[PubMed](#)]
47. Taylor, R.A.; Phelan, P.E.; Otanicar, T.P.; Adrian, R.; Prasher, R. Nanofluid optical property characterization: Towards efficient direct absorption solar collectors. *Nanoscale Res. Lett.* **2011**, *6*, 225. [[CrossRef](#)] [[PubMed](#)]
48. Fang, J.; Xuan, Y. Investigation of optical absorption and photothermal conversion characteristics of binary CuO/ZnO nanofluids. *RSC Adv.* **2017**, *7*, 56023–56033. [[CrossRef](#)]
49. Qu, J.; Tian, M.; Han, X.; Zhang, R.; Wang, Q. Photo-thermal conversion characteristics of MWCNT-H₂O nanofluids for direct solar thermal energy absorption applications. *Appl. Therm. Eng.* **2017**, *124*, 486–493. [[CrossRef](#)]
50. Zhang, L.; Chen, L.; Liu, J.; Fang, X.; Zhang, Z. Effect of morphology of carbon nanomaterials on thermo-physical characteristics, optical properties and photo-thermal conversion performance of nanofluids. *Renew. Energy* **2016**, *99*, 888–897. [[CrossRef](#)]
51. He, Q.; Wang, S.; Zeng, S.; Zheng, Z. Experimental investigation on photothermal properties of nanofluids for direct absorption solar thermal energy systems. *Energy Convers. Manag.* **2013**, *73*, 150–157. [[CrossRef](#)]

52. Li, X.; Zeng, G.; Lei, X. The stability, optical properties and solar-thermal conversion performance of SiC-MWCNTs hybrid nanofluids for the direct absorption solar collector (DASC) application. *Sol. Energy Mater. Sol. Cells* **2020**, *206*, 110323. [[CrossRef](#)]
53. Du, M.; Tang, G. Optical property of nanofluids with particle agglomeration. *Sol. Energy* **2015**, *122*, 864–872. [[CrossRef](#)]
54. Meng, Z.; Li, Y.; Chen, N.; Wu, D.; Zhu, H. Broad-band absorption and photo-thermal conversion properties of zirconium carbide aqueous nanofluids. *J. Taiwan Inst. Chem. Eng.* **2017**, *80*, 286–292. [[CrossRef](#)]
55. Zhu, L.; Gao, M.; Peh, C.K.N.; Ho, G.W.W. Solar-driven photothermal nanostructured materials designs and prerequisites for evaporation and catalysis applications. *Mater. Horiz.* **2018**, *5*, 323–343. [[CrossRef](#)]
56. Li, X.; Chen, W.; Zou, C. An experimental study on β -cyclodextrin modified carbon nanotubes nanofluids for the direct absorption solar collector (DASC): Specific heat capacity and photo-thermal conversion performance. *Sol. Energy Mater. Sol. Cells* **2020**, *204*, 110240. [[CrossRef](#)]
57. Hashim, A.M.; Rashid, F.; Fayyadh, I.K. Preparation of Nanofluid (Al_2O_3 -water) for Energy Storage. *IOSR J. Appl. Chem.* **2013**, *5*, 48–49. [[CrossRef](#)]
58. Xuan, Y.; Duan, H.; Li, Q. Enhancement of solar energy absorption using a plasmonic nanofluid based on TiO_2/Ag composite nanoparticles. *RSC Adv.* **2014**, *4*, 16206–16213. [[CrossRef](#)]
59. Filho, E.P.B.; Mendoza, O.S.H.; Beicker, C.L.L.; Menezes, A.; Wen, D. Experimental investigation of a silver nanoparticle-based direct absorption solar thermal system. *Energy Convers. Manag.* **2014**, *84*, 261–267. [[CrossRef](#)]
60. Liu, J.; Ye, Z.; Zhang, L.; Fang, X.; Zhang, Z. A combined numerical and experimental study on graphene/ionic liquid nanofluid based direct absorption solar collector. *Sol. Energy Mater. Sol. Cells* **2015**, *136*, 177–186. [[CrossRef](#)]
61. Chen, M.; He, Y.; Zhu, J.; Shuai, Y.; Jiang, B.; Huang, Y. An experimental investigation on sunlight absorption characteristics of silver nanofluids. *Sol. Energy* **2015**, *115*, 85–94. [[CrossRef](#)]
62. Meng, Z.; Wu, D.; Wang, L.; Zhu, H.; Li, Q. Carbon nanotube glycol nanofluids: Photo-thermal properties, thermal conductivities and rheological behavior. *Particuology* **2012**, *10*, 614–618. [[CrossRef](#)]
63. Boldoo, T.; Ham, J.; Cho, H. Experimental investigation of the photo-thermal conversion performance of Fe_3O_4 nanofluid under a magnetic field. *Int. J. Nanotechnol.* **2019**, *16*, 244. [[CrossRef](#)]
64. Zeng, J.; Xuan, Y. Tunable full-spectrum photo-thermal conversion features of magnetic-plasmonic $\text{Fe}_3\text{O}_4/\text{TiN}$ nanofluid. *Nano Energy* **2018**, *51*, 754–763. [[CrossRef](#)]
65. Verma, S.K.; Tiwari, A.K.; Tripathi, M. An evaluative observation on impact of optical properties of nanofluids in performance of photo-thermal concentrating systems. *Sol. Energy* **2018**, *176*, 709–724. [[CrossRef](#)]
66. Chen, L.; Xu, C.; Liu, J.; Fang, X.; Zhang, Z. Optical absorption property and photo-thermal conversion performance of graphene oxide/water nanofluids with excellent dispersion stability. *Sol. Energy* **2017**, *148*, 17–24. [[CrossRef](#)]
67. Liu, J.; Xu, C.; Chen, L.; Fang, X.; Zhang, Z. Preparation and photo-thermal conversion performance of modified graphene/ionic liquid nanofluids with excellent dispersion stability. *Sol. Energy Mater. Sol. Cells* **2017**, *170*, 219–232. [[CrossRef](#)]
68. Boldoo, T.; Ham, J.; Cho, H. Comparison Study on Photo-Thermal Energy Conversion Performance of Functionalized and Non-Functionalized MWCNT Nanofluid. *Energies* **2019**, *12*, 3763. [[CrossRef](#)]
69. Nagarajan, P.; Subramani, J.; Suyambazhahan, S.; Sathyamurthy, R. Nanofluids for Solar Collector Applications: A Review. *Energy Procedia* **2014**, *61*, 2416–2434. [[CrossRef](#)]
70. Kim, H.; Kim, J.; Cho, H. Review of Thermal Performance and Efficiency in Evacuated Tube Solar Collector with Various Nanofluids. *Int. J. Air-Cond. Refrig.* **2017**, *25*, 1730001. [[CrossRef](#)]
71. Kalogirou, S.A. Solar thermal collectors and applications. *Prog. Energy Combust. Sci.* **2004**, *30*, 231–295. [[CrossRef](#)]
72. Tyagi, H.; Phelan, P.E.; Prasher, R. Predicted Efficiency of a Low-Temperature Nanofluid-Based Direct Absorption Solar Collector. *J. Sol. Energy Eng.* **2009**, *131*, 041004. [[CrossRef](#)]
73. Kim, H.; Ham, J.; Park, C.; Cho, H. Theoretical investigation of the efficiency of a U-tube solar collector using various nanofluids. *Energy* **2016**, *94*, 497–507. [[CrossRef](#)]
74. Saffarian, M.R.; Moravej, M.; Doranehgard, M.H. Heat transfer enhancement in a flat plate solar collector with different flow path shapes using nanofluid. *Renew. Energy* **2020**, *146*, 2316–2329. [[CrossRef](#)]

75. Hussein, O.A.; Habib, K.; Muhsan, A.S.; Saidur, R.; Alawi, O.A.; Ibrahim, T.K. Thermal performance enhancement of a flat plate solar collector using hybrid nanofluid. *Sol. Energy* **2020**, *204*, 208–222. [[CrossRef](#)]
76. Tong, Y.; Chi, X.; Kang, W.; Cho, H. Comparative investigation of efficiency sensitivity in a flat plate solar collector according to nanofluids. *Appl. Therm. Eng.* **2020**, *174*, 115346. [[CrossRef](#)]
77. Kang, W.; Shin, Y.; Cho, H. Experimental investigation on the heat transfer performance of evacuated tube solar collector using CuO nanofluid and water. *J. Mech. Sci. Technol.* **2019**, *33*, 1477–1485. [[CrossRef](#)]
78. Kim, H.; Kim, J.; Cho, H. Experimental study on performance improvement of U-tube solar collector depending on nanoparticle size and concentration of Al₂O₃ nanofluid. *Energy* **2017**, *118*, 1304–1312. [[CrossRef](#)]
79. Tong, Y.; Lee, H.; Kang, W.; Cho, H. Energy and exergy comparison of a flat-plate solar collector using water, Al₂O₃ nanofluid, and CuO nanofluid. *Appl. Therm. Eng.* **2019**, *159*, 113959. [[CrossRef](#)]
80. Yurddaş, A. Optimization and thermal performance of evacuated tube solar collector with various nanofluids. *Int. J. Heat Mass Transf.* **2020**, *152*, 119496. [[CrossRef](#)]
81. Razali, N.F.M.; Fudholi, A.; Ruslan, M.H.; Sopian, K. Review of water-nanofluid based photovoltaic/thermal (PV/T) systems. *Int. J. Electr. Comput. Eng. (IJECE)* **2019**, *9*, 134–140. [[CrossRef](#)]
82. Sardarabadi, M.; Passandideh-Fard, M.; Heris, S.Z. Experimental investigation of the effects of silica/water nanofluid on PV/T (photovoltaic thermal units). *Energy* **2014**, *66*, 264–272. [[CrossRef](#)]
83. Ghadiri, M.; Sardarabadi, M.; Pasandideh-Fard, M.; Moghadam, A.J. Experimental investigation of a PVT system performance using nano ferrofluids. *Energy Convers. Manag.* **2015**, *103*, 468–476. [[CrossRef](#)]
84. Cui, Y.; Zhu, Q. Study of Photovoltaic/Thermal Systems with MgO-Water Nanofluids Flowing over Silicon Solar Cells. In Proceedings of the 2012 Asia-Pacific Power and Energy Engineering Conference, Shanghai, China, 27–29 March 2012.
85. Jing, D.; Hu, Y.; Liu, M.; Wei, J.; Guo, L. Preparation of highly dispersed nanofluid and CFD study of its utilization in a concentrating PV/T system. *Sol. Energy* **2015**, *112*, 30–40. [[CrossRef](#)]
86. Shirazi, A.; Otanicar, T.; Rosengarten, G. Nanofluid-based optical filter optimization for PV/T systems. *Light. Sci. Appl.* **2012**, *1*, e34. [[CrossRef](#)]
87. Zhu, M.; Li, Y.; Chen, G.; Jiang, F.; Yang, Z.; Luo, X.; Wang, Y.; Lacey, S.D.; Dai, J.; Wang, C.; et al. Tree-Inspired Design for High-Efficiency Water Extraction. *Adv. Mater.* **2017**, *29*. [[CrossRef](#)] [[PubMed](#)]
88. Kim, S.; Piao, G.; Han, D.S.; Shon, H.K.; Park, H. Solar desalination coupled with water remediation and molecular hydrogen production: A novel solar water-energy nexus. *Energy Environ. Sci.* **2018**, *11*, 344–353. [[CrossRef](#)]
89. Neumann, O.; Neumann, A.D.; Tian, S.; Thibodeaux, C.; Shubhankar, S.; Müller, J.; Silva, E.; Alabastri, A.; Bishnoi, S.W.; Nordlander, P.; et al. Combining Solar Steam Processing and Solar Distillation for Fully Off-Grid Production of Cellulosic Bioethanol. *ACS Energy Lett.* **2016**, *2*, 8–13. [[CrossRef](#)]
90. Wang, Z.; Liu, Y.; Tao, P.; Shen, Q.; Yi, N.; Zhang, F.; Liu, Q.; Song, C.; Zhang, D.; Shang, W.; et al. Bio-Inspired Evaporation Through Plasmonic Film of Nanoparticles at the Air-Water Interface. *Small* **2014**, *10*, 3234–3239. [[CrossRef](#)]
91. Sajadi, S.M.; Farokhnia, N.; Irajizad, P.; Hasnain, M.; Ghasemi, H. Flexible artificially-networked structure for ambient/high pressure solar steam generation. *J. Mater. Chem. A* **2016**, *4*, 4700–4705. [[CrossRef](#)]
92. Liu, X.; Huang, J.; Wang, X.; Cheng, G.; He, Y. Investigation of graphene nanofluid for high efficient solar steam generation. *Energy Procedia* **2017**, *142*, 350–355. [[CrossRef](#)]
93. Dao, V.-D.; Choi, H.-S. Carbon-Based Sunlight Absorbers in Solar-Driven Steam Generation Devices. *Glob. Chall.* **2018**, *2*, 1700094. [[CrossRef](#)]
94. Huang, J.; He, Y.; Chen, M.; Wang, X. Separating photo-thermal conversion and steam generation process for evaporation enhancement using a solar absorber. *Appl. Energy* **2019**, *236*, 244–252. [[CrossRef](#)]
95. Wang, G.; Fu, Y.; Ma, X.; Pi, W.; Liu, D.; Wang, X. Reusable reduced graphene oxide based double-layer system modified by polyethylenimine for solar steam generation. *Carbon* **2017**, *114*, 117–124. [[CrossRef](#)]
96. Huang, J.; He, Y.; Hu, Y.; Wang, X. Steam generation enabled by a high efficiency solar absorber with thermal concentration. *Energy* **2018**, *165*, 1282–1291. [[CrossRef](#)]
97. Fu, Y.; Mei, T.; Wang, G.; Guo, A.; Dai, G.; Wang, S.; Wang, J.; Li, J.; Wang, X. Investigation on enhancing effects of Au nanoparticles on solar steam generation in graphene oxide nanofluids. *Appl. Therm. Eng.* **2017**, *114*, 961–968. [[CrossRef](#)]

98. Wang, X.; He, Y.; Liu, X.; Cheng, G.; Zhu, J. Solar steam generation through bio-inspired interface heating of broadband-absorbing plasmonic membranes. *Appl. Energy* **2017**, *195*, 414–425. [[CrossRef](#)]
99. Liu, X.; Wang, X.; Huang, J.; Cheng, G.; He, Y. Volumetric solar steam generation enhanced by reduced graphene oxide nanofluid. *Appl. Energy* **2018**, *220*, 302–312. [[CrossRef](#)]
100. Zeiny, A.; Jin, H.; Lin, G.; Song, P.; Wen, D. Solar evaporation via nanofluids: A comparative study. *Renew. Energy* **2018**, *122*, 443–454. [[CrossRef](#)]

Publisher’s Note: MDPI stays neutral with regard to jurisdictional claims in published maps and institutional affiliations.



© 2020 by the authors. Licensee MDPI, Basel, Switzerland. This article is an open access article distributed under the terms and conditions of the Creative Commons Attribution (CC BY) license (<http://creativecommons.org/licenses/by/4.0/>).